isvr Institute of Sound and Vibration Research

Measurement of Flexural Propagating Waves in Pipes using Shaped PVDF Modal Sensors

W. Variyart and M.J. Brennan

ISVR Technical Memorandum 847

November 1999

University of Southampton

SCIENTIFIC PUBLICATIONS BY THE ISVR

Technical Reports are published to promote timely dissemination of research results by ISVR personnel. This medium permits more detailed presentation than is usually acceptable for scientific journals. Responsibility for both the content and any opinions expressed rests entirely with the author(s).

Technical Memoranda are produced to enable the early or preliminary release of information by ISVR personnel where such release is deemed to the appropriate. Information contained in these memoranda may be incomplete, or form part of a continuing programme; this should be borne in mind when using or quoting from these documents.

Contract Reports are produced to record the results of scientific work carried out for sponsors, under contract. The ISVR treats these reports as confidential to sponsors and does not make them available for general circulation. Individual sponsors may, however, authorize subsequent release of the material.

UNIVERSITY OF SOUTHAMPTON

INSTITUTE OF SOUND AND VIBRATION RESEARCH

DYNAMICS GROUP

Measurement of Flexural Propagating Waves in Pipes using Shaped PVDF Modal Sensors

by

W. Variyart and M.J. Brennan

ISVR Technical Memorandum No. 847

November 1999

Authorized for issue by
Dr. M.J. Brennan
Group Chairman

Abstract

In pipe vibration the n=2 (ovalling mode) wave causes a large increase of strain in the pipe wall at the cut-on frequency when the wave starts to propagate. Hence from a fatigue perspective this wave is of major concern. In this report the design of a shaped PVDF modal sensor to target this wave is investigated.

Based on Flugge's shell theory, the relationship between the charge generated from a PVDF sensor and the combination of the axial and circumferential bending strains is established for the case of in-extensional deformation. It is found that a practical modal sensor is sensitive to higher order modes as well as the n=2 mode. This cross-sensitivity is dependent upon the width of the modal sensor. It is found that, if the width is small enough to keep the axial strain constant over its surface, the modal sensor will only be sensitive to the circumferential bending strain of the pipe and hence to the n = 2 mode. For the axial strain of n = 2 mode to be constant over the frequency range of interest, the width of the modal sensor has to be less than one third of the wavelength of the flexural wave at the ring frequency and hence it only senses the response of the n = 2 mode. Since the orientation of the n=2 mode shape at some arbitrary point on the pipe is unknown, two elements to the sensor are required that independently measure the cosine and sine components of the wave.

Theoretical predictions of the modal sensor were successfully validated by some experimental work. The effectiveness of the sensor was also experimentally compared with an array of accelerometers.

CONTENTS

Nomenclature

u is the axial component of the displacement

v is the tangential component of the displacement

w is the radial component of the displacement

U is the axial amplitude

V is the tangential amplitude

W is the radial amplitude

$\overline{\overline{W}}$ is the radial displacement in the frequency domain

$\overline{U}$ is the axial amplitude in the wavenumber domain

$\overline{V}$ is the tangential amplitude in the wavenumber domain

$\overline{W}$ is the radial amplitude in the wavenumber domain

a is the radius of the pipe

h is the thickness of the pipe

h_{pv} is the thickness of the PVDF,

$z_o = (h + h_{pv})/2$ is the distance from the mid-plane of the pipe to that of the PVDF,

$s = x/a$ is the non-dimensional length

s_c is the non-dimensional axial location of centre of the sensor to the radius of the pipe,

b_s is the ratio of a half of width of the sensor to the radius of the pipe,

$\beta = \dfrac{h}{a\sqrt{12}}$ is the wall thickness ratio of the pipe

$c_L = \sqrt{\dfrac{E}{\rho(1-\nu^2)}}$ is the longitudinal wave velocity in the pipe

E is the Young's modulus of the pipe

E_{pv} is Young's modulus of PVDF

ρ is the density of the pipe

ν is the Poisson's ratio of the pipe

ν_{pv} is Poisson's ratio of PVDF

η is the loss factor of the pipe

$\omega = 2\pi f$ is the circular frequency

$\Omega = a\omega/c_L$ is the normalised frequency to the ring frequency, c_L/a

n is the mode number

k_{nb} is the non-dimensional branch axial wavenumber (the axial wavenumber is multiplied by the radius of the pipe)

ϕ is the azimuthal orientation angle of the pipe with respect to the excitation force

θ is the azimuthal angle of the pipe

$F(s,\theta,t)$ is the force per unit area

F_o is the amplitude of the point force

d_{31} and d_{32} are the piezoelectric strain constants.

e_{31} and e_{32} are the piezoelectric stress constants.

S_x and S_θ are the axial and circumferential strains, respectively,

Y_n is the mobility of the pipe of the n^{th} mode

H_n is the accelerance of the pipe of the n^{th} mode

q_t is the total generated charge of the modal sensor

q_s is the total generated charge of the modal sensor shaped in the sine function

q_c is the total generated charge of the modal sensor shaped in the cosine function

1. INTRODUCTION

In many processing and chemical industries, and in ships and aircraft, pipework is important for transporting fluids, i.e. gas, cooling water and hydraulic fluid. A piping system can be excited by many sources connected to the structure or internal fluid such as compressors, pumps, or valves. The vibrational energy propagating along a piping system can excite other devices attached to the structure and it frequently causes excessive noise radiation and may result in failure of the system due to fatigue. To control the vibration of the pipe, a thorough understanding of the dynamic behaviour of fluid-filled shells is needed since it is critical in an investigation of active vibration control applied to such systems.

The theories of thin cylindrical shells have been developed mostly on the basis of the strain action and with the aid of certain simplifying assumptions. There are small differences between the various theories depending on their assumptions and the main theories are described by Leissa [1].

Unlike a one-dimensional structure such as a beam and bar or two-dimensional structure such as a plate, the dynamic behaviour of a three-dimensional structure such as a pipe is more complex, particular when it contains fluid. There is some work to explain this phenomenon in terms of dispersion curves, such as the work done by Lin and Morgan [2], who used the concept of a rigid tube and an infinitely flexible tube to construct a curve of phase velocity. With this curve, the behaviour of the pipe can be explained in terms of that of a bar, a beam and a plate. They concluded that all the modes except the first two modes have a minimum cut-on frequency and the first two modes exist at all frequencies. However, this work was limited to consider only real wave types. Similarly, Fuller and Fahy [3] presented a complete set of dispersion curves based on Donnell-Mushtari shell theory. All of the wave types were considered and discussed in their paper. Moreover, the energy distribution between the structure and contained fluid was derived and discussed. It may be considered as the basic formula of the energy interchange between the structure and the fluid. Based on such research, later work by Fuller [4] considered the energy distribution in the case of the shell excited by a radial line force and by a point force. Using the theory of residues, he also presented the transfer mobility of an infinite fluid-filled shell excited by a radial line force. A simple form of the point mobility based on Cremer's expression for the shell was

proposed by Heckl [5]. The physical interpretation of the dynamic behaviour of a pipe in vacuo and with contained fluid was clearly described by Brennan et al [6]. Using phase velocity and dispersion curves based on Kennard shell theory, the behaviour of individual waves propagating along the shell can be described in terms of the flexural beam-like, plate-like bending, longitudinal, torsional waves and acoustic waves in a duct.

Once the behaviour of the pipe is known, it is possible to control the vibration occurring on the pipe. One of the elements, which plays an important role in an active vibration control system, is a sensor, which may be classified as discrete point sensors such as accelerometers or strain gauges and distributed sensors such as piezoelectric materials. The piezoelectric materials used as sensors employ the direct piezoelectric effect, which converts structural motion into electricity. They are commercially available as PZT (lead zirconate titanate) and PVDF (Polyvinylidene fluoride). Both of them can be manufactured in many shapes so that they can readily be integrated into structures by embedding or bonding them, and this gives them advantages over discrete point sensors.

In addition, since the discrete point sensor/actuator detects/excites all modes including the residual modes (undesired modes), they cause spillover in controlling vibration (Balas [7]). This problem may be overcome by using modal sensors/actuators, which only sense/excite the desired modes.

The modal sensor was firstly introduced by Lee and Moon [8], who applied it on a beam, and included an analysis of the modal sensor for a plate as well. It was extended in theory and practice for a plate by Gu et al [9]. The analysis of a PVDF sensor bonded to a shell was developed by Tzou [10]. The effect of many factors to the output of the segmented PVDF, i.e. thickness of the PVDF and shell, the curvature of the shell, was investigated by Tzou and Bao [11]. However, the sensors in both pieces of work were not discussed in the context of a modal sensor. Since the circumferential mode shapes of a pipe are in the form of sine and cosine functions, then from the work by Lee and Moon [8] the shapes of the modal sensors should take the form of sine and cosine functions as well. The modal sensor for an infinitely long pipe following such shapes were used in the work of Fuller and Brevart [12]. Since, the shapes of the modal sensors need to be accurate; otherwise they cannot be used in an active control system to completely cancel

undesired modes, Callahan and Baruh [13] preferred to use segmented PVDFs (rectangular shape) with the sensor output cancellation technique. By using a number of sensors and decreasing the magnitude of the real part of the observer gain, then the sensor output converges to the desired mode. However, this method risks the ill-conditioning of the modal coordinate matrix and it takes some time to converge to the desired mode. Therefore, the modal sensor for the pipe in the work reported here still uses the PVDF in the form of sine and cosine functions. The main aim of this work is to investigate the use of a distributed sensor to discriminate against the n = 2 circumferential propagating mode in a pipe.

In the current work, two main expressions are presented. The first is the dispersion equation based on the simplified version of the Flugge shell theory, which is derived with the assumption that the wall thickness is thin, the frequency range of interest is below the ring frequency and the very long axial wavelength is neglected. Based on this work, the frequency equation and the radial transfer mobility of the pipe in vacuo are established. In addition, the modal decomposition for an array of accelerometers based on discrete orthogonality is also presented and a general expression of a circumferential mode sensor is derived. Subsequent work concentrates on a modal sensor for the n = 2 mode and this is validated experimentally.

2. IN VACUO SHELL THEORY

2.1 Introduction

It is well-known that the motion of a pipe is complicated since its structure is three dimensional. For a thin walled pipe, structural waves propagate in the axial direction along a pipe and in a circumferential direction to form a helical pattern as shown in fig 2.1 (Fahy [14]). The wavenumber of the helical wave, k_{cs}, is the vector combination of the waveguide components in both directions, the axial wavenumber, k_{nb}, and circumferential wavenumber, k_c, which gives

$$k_{cs}^2 = k_{nb}^2 + k_c^2$$

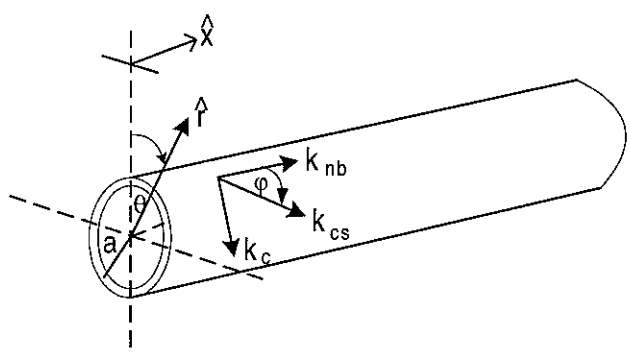

Figure 2.1: Diagram showing a semi-infinite cylinder and axial, circumferential and helical wavenumbers

The axial wavenumber is thus given by

$$k_{nb} = \sqrt{k_{cs}^2 - k_c^2}$$

It can be seen that k_{nb} is only real and hence propagating when $k_{cs}^2 \geq k_c^2$. Otherwise, the wave is evanescent.

Due to the closure of the pipe in the circumferential direction, the wave propagation must be continuous in this direction and hence, the circumferential characteristic takes the form of sine or cosine functions of $k_c a\theta$, where $k_c = n/a$, n is the mode number, a is the radius of a pipe and θ is the angle between the wavevectors. With the form of such a function in the circumferential direction, at n= 0 (also known as the breathing mode)

there is only stretching or contracting of the pipe wall, while at n = 1 or bending mode, the pipe cross section is undeformed.

There are many shell theories based on the strain at a point to explain the motion of a pipe wall but none of these theories is universally accepted due to small differences between them. This arises from the different assumptions. Usually, most theories are based on the assumption of zero normal shear strain. Nowadays, the versions of shell theories generally used by researchers are Donnell-Mushtari, Love, Timoshenko, Kennard and Flugge (Leissa [1]).

In this work, a simplified theory based on Flugge shell theory with some additional assumptions is developed and the point-forced mobility and accelerance of a thin-walled pipe are derived.

2.2 Simplified Version of Flugge Shell Theory in vacuo

Due to the complicated form of shell theories, it is difficult to apply them to the vibration problems of an infinitely long pipe, i.e. the dispersion equation and the point/transfer mobility of a pipe. So, in this section it is intended to derive a simple form of the dispersion equation based on Flugge shell theory. Once the simplified equation is established, the simple formula of the mobility of a pipe can easily be determined.

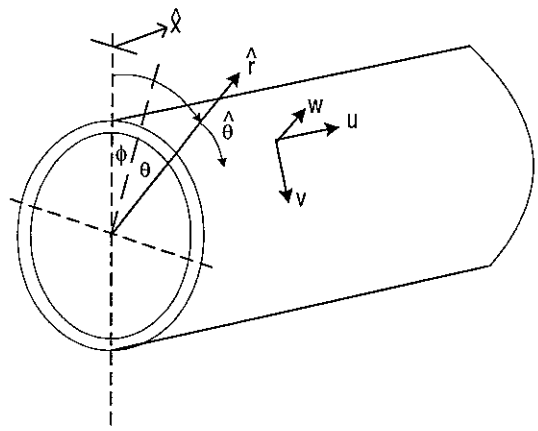

Figure 2.2: Cylindrical coordinate system for a pipe.

In the derivation, it is assumed that the wall thickness is thin compared to the radius of the pipe, the frequency range of interest is below the ring frequency and the very long axial wavelength is neglected.

A schematic of the cylindrical coordinate system for the pipe is shown in figure 2.2 where $\hat{r}, \hat{\theta}$ and $\hat{x}$ are the unit vectors. Since the circumferential reference position on a pipe is unknown, the orientation angle, ϕ, is defined. The equation of motion of free vibration of the pipe is given by (Leissa [1])

$$\Im \begin{bmatrix} u \\ v \\ w \end{bmatrix} = 0 \qquad \ldots(2.1)$$

where

$$\Im = \begin{bmatrix} \left(\frac{\partial^2}{\partial s^2} + \frac{(1-\nu)}{2}(1+\beta^2)\frac{\partial^2}{\partial \theta^2} - \frac{\rho(1-\nu^2)a^2}{E}\frac{\partial^2}{\partial t^2}\right) & \left(\frac{(1+\nu)}{2}\frac{\partial^2}{\partial s \partial \theta}\right) & \left(\nu\frac{\partial}{\partial s} - \beta^2\frac{\partial^3}{\partial s^3} + \beta^2\frac{(1-\nu)}{2}\frac{\partial^3}{\partial s \partial \theta^2}\right) \\ \left(\frac{(1+\nu)}{2}\frac{\partial^2}{\partial s \partial \theta}\right) & \left(\frac{(1-\nu)}{2}(1+3\beta^2)\frac{\partial^2}{\partial s^2} + \frac{\partial^2}{\partial \theta^2} - \frac{\rho(1-\nu^2)a^2}{E}\frac{\partial^2}{\partial t^2}\right) & \left(\frac{\partial}{\partial \theta} - \beta^2\frac{(3-\nu)}{2}\frac{\partial^3}{\partial s^2 \partial \theta}\right) \\ \left(\nu\frac{\partial}{\partial s} - \beta^2\frac{\partial^3}{\partial s^3} + \beta^2\frac{(1-\nu)}{2}\frac{\partial^3}{\partial s \partial \theta^2}\right) & \left(\frac{\partial}{\partial \theta} - \beta^2\frac{(3-\nu)}{2}\frac{\partial^3}{\partial s^2 \partial \theta}\right) & \left(1 + \beta^2\nabla^4 + \beta^2 + 2\beta^2\frac{\partial^2}{\partial \theta^2} + \frac{\rho(1-\nu^2)a^2}{E}\frac{\partial^2}{\partial t^2}\right) \end{bmatrix}$$

where $\nabla^4 = \nabla^2\nabla^2$ and

$$\nabla^2 = \frac{\partial^2}{\partial s^2} + \frac{\partial^2}{\partial \theta^2}$$

So, $$\nabla^4 = \frac{\partial^4}{\partial s^4} + \frac{\partial^4}{\partial \theta^4} + \frac{\partial^4}{\partial s^2 \partial \theta^2}$$

The solution of the equation of motion of an infinite pipe may be written as

$$\begin{aligned} u(s,\theta,t) &= \sum_{n=0}^{\infty}\sum_{b=1}^{8} U_{nb}\cos(n(\theta-\phi))e^{j(k_{nb}s-\pi/2-\omega t)} \\ v(s,\theta,t) &= \sum_{n=0}^{\infty}\sum_{b=1}^{8} V_{nb}\sin(n(\theta-\phi))e^{j(k_{nb}s-\omega t)} \\ w(s,\theta,t) &= \sum_{n=0}^{\infty}\sum_{b=1}^{8} W_{nb}\cos(n(\theta-\phi))e^{j(k_{nb}s-\omega t)} \end{aligned} \qquad \ldots(2.2)$$

where ϕ is the azimuthal orientation angle and

θ is the azimuthal angle.

Substitution of the displacements of equation (2.2) into the equation (2.1) yields

$$\begin{bmatrix} L_{11} & L_{12} & L_{13} \\ L_{21} & L_{22} & L_{23} \\ L_{31} & L_{32} & L_{33} \end{bmatrix} \begin{bmatrix} U_n \\ V_n \\ W_n \end{bmatrix} = 0 \qquad \ldots(2.3)$$

where

$$L_{11} = k_{nb} + \frac{(1-\nu)}{2}\left(1+\beta^2\right)n^2 - \Omega^2$$

$$L_{12} = \frac{(1+\nu)}{2} n k_{nb}$$

$$L_{13} = \nu k_{nb} + \beta^2 k_{nb}^3 - \frac{(1-\nu)}{2}\beta^2 n^2 k_{nb}$$

$$L_{21} = L_{12}$$

$$L_{22} = \frac{(1-\nu)}{2}(1+3\beta^2)k_{nb}^2 + n^2 - \Omega^2$$

$$L_{23} = n + \frac{(3-\nu)}{2}\beta^2 n k_{nb}^2$$

$$L_{31} = L_{13}$$

$$L_{32} = L_{23}$$

$$L_{33} = 1+\beta^2 + \beta^2(k_{nb}^2 + n^2)^2 - 2\beta^2 n^2 - \Omega^2$$

The non-dimensional wavenumber, k_{nb}, of the thin walled pipe in vacuo can be determined from

$$\text{Det}|L| = 0 \qquad \ldots(2.4)$$

The determinant of matrix L is arranged with terms involving β grouped together and since for a thin pipe $\beta^2 << 1$, then the higher order terms of β (i.e. β^4 and β^6) can be neglected. Thus, the result of the determinant of the matrix L becomes

$$\frac{1}{8}\beta^2\left[\left\{4(1-\nu)(k_{nb}^2+n^2)^2(k_{nb}^2+n^2-1)^2+8(1-\nu)^2\left(k_{nb}^4-n^2\left(n^2-1\right)\right)k_{nb}^2+12(1-\nu)^2(1+\nu)k_{nb}^4\right\}\right.$$
$$\left.-\Omega^2\left\{4(3-\nu)(k_{nb}^2+n^2)(k_{nb}^2+n^2-1)^2+4(1-\nu)(k_{nb}^2+n^2)(k_{nb}^2+n^2+1)+8(1-\nu)(4k_{nb}^2+1)k_{nb}^2\right\}\right.$$
$$-\frac{1}{2}\Omega^2\left[(1-\nu)(k_{nb}^2+n^2)(k_{nb}^2+n^2+1)+2(1-\nu^2)k_{nb}^2\right]+\frac{1}{2}(1-\nu)^2(1+\nu)k_{nb}^4+\frac{1}{2}(3-\nu)(k_{nb}^2+n^2)\Omega^4$$
$$+\Omega^4-\Omega^6=0$$

...(2.5)

Apart from the assumption of $\beta^2 << 1$, another assumption is that $1/k_{nb}^2 >> \beta^2$. This is reasonable for a thin walled pipe since $\beta^2 \approx 2.1\text{x}10^{-4}$ for h/a = 0.05 while k_{nb} increases from zero to about 6 in the non-dimensional frequency range of zero to one (provided by the dispersion curve in the next section). Since $k_{nb} = 2\pi a/\lambda_{nb}$, where λ_{nb} is a branch axial wavelength, and $\beta = h/\sqrt{12}\,a$, the assumption can be expressed as, $\lambda_{nb} >> \pi h/\sqrt{3} \approx 2h$. Physically, it implies that waves, whose non-dimensional axial wavenumber is smaller than two times of the wall thickness, are neglected. Since higher frequencies mean smaller axial wavelengths, the above assumption also means that the very high frequency range is neglected. After applying these two assumptions equation (2.5) becomes

$$\frac{1}{2}\beta^2\left[(1-\nu)(k_{nb}^2+n^2)^2(k_{nb}^2+n^2-1)^2-(3-\nu)(k_{nb}^2+n^2)(k_{nb}^2+n^2-1)^2\Omega^2\right]$$
$$-\frac{1}{2}\Omega^2\left[(1-\nu)(k_{nb}^2+n^2)(k_{nb}^2+n^2+1)+2(1-\nu^2)k_{nb}^2\right]+\frac{1}{2}(1-\nu)^2(1+\nu)k_{nb}^4+\frac{1}{2}(3-\nu)(k_{nb}^2+n^2)\Omega^4$$
$$+\Omega^4-\Omega^6=0$$

...(2.6)

At high frequencies, where $\Omega > 1$, equation (2.6) can be used to determined the non-dimensional wavenumber, but, in the frequency range of interest limited below the ring frequency, where $\Omega < 1$, the high order terms of Ω (i.e. Ω^4 and Ω^6) including the term containing the product of β^2 and Ω^2 are very small value and thus they can be ignored. Therefore, at the frequencies below the ring frequency ($\Omega < 1$), equation (2.6) becomes

$$\frac{1}{2}\beta^2(1-\nu)(k_{nb}^2+n^2)^2(k_{nb}^2+n^2-1)^2-\frac{1}{2}\Omega^2\left[(1-\nu)(k_{nb}^2+n^2)(k_{nb}^2+n^2+1)+2(1-\nu^2)k_{nb}^2\right]$$
$$+\frac{1}{2}(1-\nu)^2(1+\nu)k_{nb}^4=0$$

...(2.7)

Moreover, the assumption of $k_{nb}^2 >> \Omega^2$ physically means that some motions with very long axial wavelengths are not important to the total motion of the pipe. In reality, this assumption is not true around cut-on frequencies since k_{nb} is zero, when Ω has a value between zero and one. The assumption requires the condition of $\frac{\partial k_{nb}}{\partial \Omega} > 1$ just after the wave is cut-on. Thus, it effects the longitudinal and torsional waves (k_{nb} is propotional to Ω for n = 0). This assumption was pointed out by Cremer (Heckl [5]), who showed that it does not result in large errors. So, compared with the term of $\frac{1}{2}(1-\nu)^2(1+\nu)k_{nb}^4$, the term of $(1-\nu^2)\Omega^2 k_{nb}^2$ can be neglected. Hence, equation (2.7) can be rewritten as

$$\frac{1}{2}\beta^2(1-\nu)(k_{nb}^2+n^2)^2(k_{nb}^2+n^2-1)^2-\frac{1}{2}\Omega^2(1-\nu)(k_{nb}^2+n^2)(k_{nb}^2+n^2+1)+\frac{1}{2}(1-\nu)^2(1+\nu)k_{nb}^4 = 0 \qquad \ldots(2.8)$$

This can be rearranged to give the relationship between the non-dimensional frequency and the axial wavenumber.

$$\Omega^2 = \frac{\beta^2(k_{nb}^2+n^2)^2(k_{nb}^2+n^2-1)^2+(1-\nu^2)k_{nb}^4}{(k_{nb}^2+n^2)(k_{nb}^2+n^2+1)} \qquad \ldots(2.9)$$

The first term on the right hand side of equation (2.9) is related to membrane strain energy and the second term is related to strain energy of the pipe-walled flexure (Fahy [14]).

The cut-on frequencies of the circumferential mode of an infinitely long pipe are determined from the equation (2.9) by setting $k_{nb} = 0$, which corresponds to an infinitely long axial wavelength. Therefore,

$$\Omega_{co}^2 = \frac{\beta^2 n^2(n^2-1)^2}{n^2+1} \qquad \ldots(2.10)$$

2.3 Numerical analysis to evaluate the simplified version

To verify the simplified version of the shell theory in vacuo, it is compared in terms of cut-on frequencies from equation (2.10) and the dispersion curve from equation (2.8) with those obtained from the version developed by Heckl [5], Kennard's shell theory used by Brevart and Fuller [15], and from Flugge shell theory (Leissa [1]). The properties of the pipe used in the comparison, which is also used in the experiment work discussed later in this report, are given from Table 2.1.

Table 2.1: Pipe data

E (N/m^2)	ρ (kg/m^3)	ν	a (mm)	h (mm)	η
$3.55*10^9$	1430	0.4	33	1.9	0.025

Comparison of cut-on frequencies of the circumferential modes

The various frequency equations of the circumferential modes for infinitely long pipes are given as follows.

The frequency equation developed by Heckl [5] is

$$\Omega_{co}^2 = \beta^2 n^4 \left[1 - \frac{1}{2}\left(\frac{1}{1-\nu}\right)\left(\frac{4-\nu}{n^2} - \frac{2+\nu}{n^4}\right)\right],$$

by Kennard (Leissa [1]) is

$$\Omega_{co}^2 = \frac{1}{2}\left\{\left[1 + \frac{2+\nu}{2(1-\nu)}\beta^2 + n^2 - \frac{4-\nu}{2(1-\nu)}\beta^2 n^2 + \beta^2 n^4\right] \mp \sqrt{1 + \frac{2+\nu}{1-\nu}\beta^2 + 2\left(1 - 3\beta^2\right)n^2 + n^4 + \frac{3(2-3\nu)}{1-\nu}\beta^2 n^4 - 2\beta^2 n^6}\right\},$$

by Flugge's theory given by Leissa [1] is

$$\Omega_{co}^2 = \frac{1}{2}\left\{1 + n^2 + \beta^2\left(n^2 - 1\right)^2 \mp \sqrt{\left[1 + n^2 + \beta^2\left(n^2 - 1\right)^2\right]^2 - 4\beta^2 n^2 (n-1)^2}\right\}$$

and in this report is given in the equation (2.10) as:

$$\Omega_{co}^2 = \frac{\beta^2 n^2 (n^2 - 1)^2}{n^2 + 1}$$

Taking the data of the pipe from table 2.1, the ring frequency of the pipe is

$$f_r = \frac{1}{2\pi a}\sqrt{\frac{E}{\rho(1-\nu)^2}}$$
$$= 8291.1 \text{ Hz.}$$

and the maximum mode number below the ring frequency can approximately be determined by (Fahy [14])

$$n_r \cong \beta^{-1/2}$$
$$= 7$$

The cut-on frequencies of the modes below the ring frequency, which are calculated from above frequency equations, are shown in table 2.2.

Table 2.2: Cut-on frequency of the circumferential modes according to various versions of the frequency equations.

Mode Number	Heckl	Kennard	Flugge	Equation (10)
2	337.5	369.8	369.8	369.8
3	1031.2	1046.1	1046.0	1045.9
4	1997.0	2006.2	2006.1	2005.3
5	3237.7	3245.5	3245.3	3243.1
6	4753.7	4762.9	4762.6	4757.5
7	6545.3	6558.5	6558.0	6548.1

Note: the cut-on frequencies for n = 0 and 1 modes are zero and the frequency equation of Heckl's version is valid for $n \geq 2$.

It is shown in table 2.2 that the simplified version (equation 2.10) is in good agreement with the main theories, that of Kennard and Flugge for the pipe used in this report. Below the ring frequency, the maximum difference of the cut-on frequency between this simplified version and the main theories is only 0.16%.

Comparison of dispersion curves

In this section, a set of dispersion curves using equation (2.8) and some versions of shell theory, Kennard and Flugge, are compared. To verify equation (2.8), the comparisons are carried out for each mode number. The results from the simulation are shown in figure 2.3.

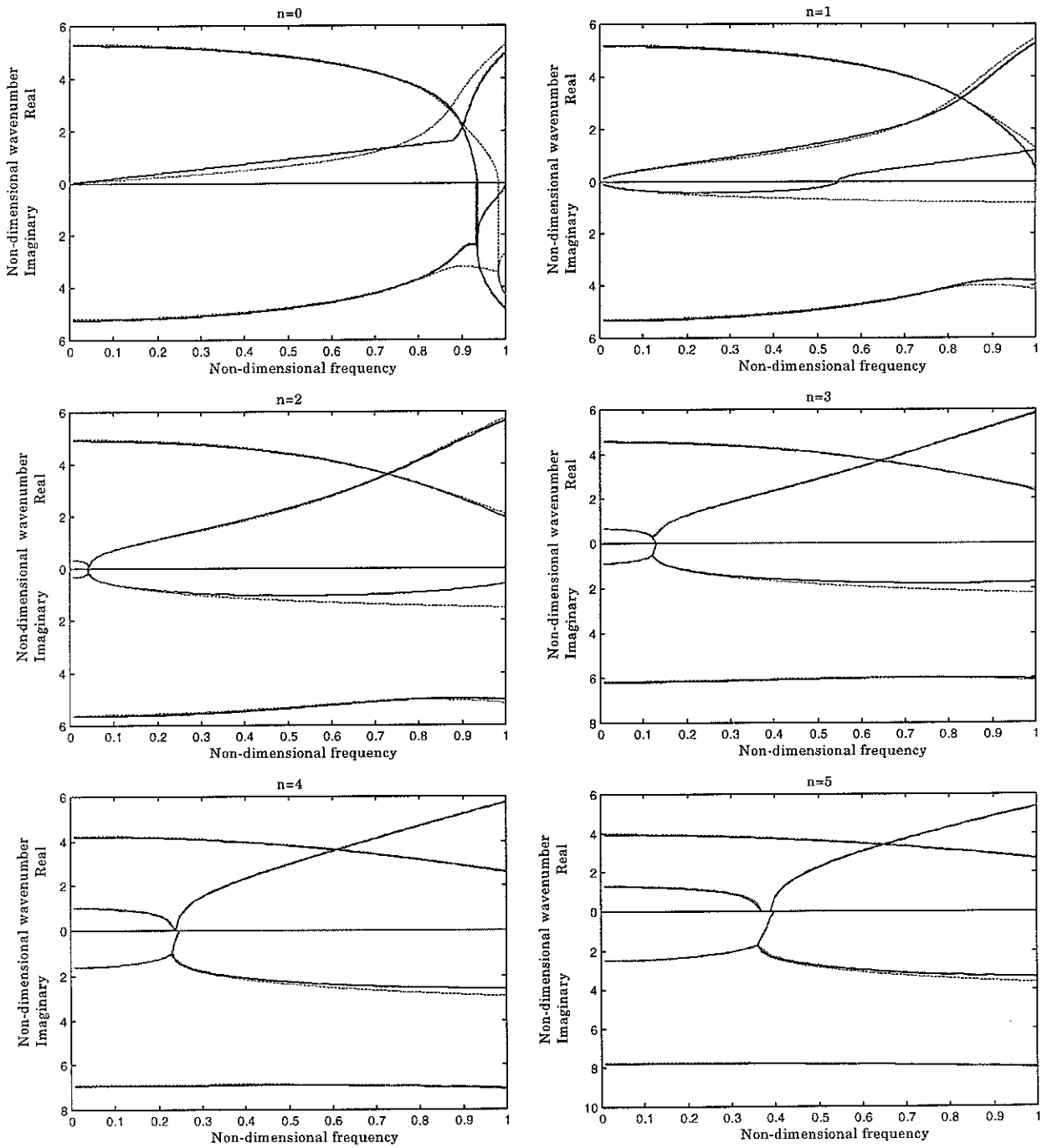

Figure 2.3. Dispersion curve of the mode number n =0 to n = 5; ..., equation (2.8); –, Kennard theory; ---, Flugge theory.

At low frequencies, all versions of shell theory are consistent. There is a small error in k_{nb} for the n= 0 mode, which has already been discussed. The assumption of $k_{nb}^2 >> \Omega^2$ has an effect on the longitudinal wave causing an error in the n= 0 mode but for $\Omega < 0.8$ it does not yield a large error. For $n \geq 1$ modes, the error occurs in the evanescent wave and increases with increasing frequency. Apart from this, below the ring frequency, all of waves types obtained from equation (2.8) are reasonably consistent with Kennard's and Flugge's shell theory.

2.4 Point force mobility of semi-infinitely long pipe

The response of a semi-infinite pipe to a point force applied at the free end is of interest in this section and is important to other analyses such as the modal decomposition and the transfer function of a modal sensor, which are presented later. A useful method to derive the response of the pipe is to analyse the point force mobility in the wavenumber domain using the spatial Fourier transform. Using residue theory and the simplified shell theory, the point force mobility of the pipe can be established in a simple form.

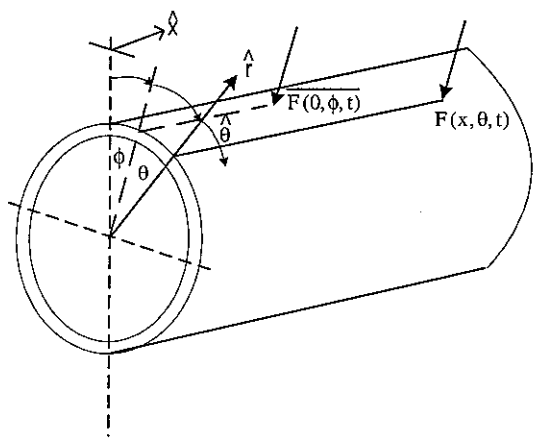

Figure 2.4. The cylindrical co-ordinate system for a semi-infinite pipe.

The cylindrical coordinate system of a pipe with an exciting point force, $\overline{F(0,\phi,t)}$, is schematically shown in figure 2.4 where $\hat{r}, \hat{\theta}$ and $\hat{x}$ are the unit vectors. As discussed in the previous section, an orientation angle, ϕ, is used to define the circumferential reference position on a pipe. The point force $\overline{F(0,\phi,t)}$ in Newtons can be expressed as a distributed force $F(s,\theta,t)$ in Newtons per square metre by (Soedel [24])

$$F(s,\theta,t)=\frac{1}{a^2}F_o\delta(s)\delta(\theta-\phi)e^{-j\omega t} \qquad \ldots(2.11)$$

where F_o is the amplitude of the point force (Newton) and

$s = x/a$.

The equation of motion of the pipe when excited by a point force in the radial direction may be written as the same form as equation (2.1) with an external force loading as (Leissa [1]):

$$\Im\begin{bmatrix}u\\v\\w\end{bmatrix}=\begin{bmatrix}0\\0\\-\dfrac{a^2(1-\nu^2)}{Eh}F(s,\theta,t)\end{bmatrix} \qquad \ldots(2.12)$$

where a is the radius of the pipe,

E is Young's modulus of the pipe and

$F(s,\theta,t)$ is the force per unit area.

The Fourier transform is used to analyse the vibration response of a pipe due to a point force and the pipe displacements may be written as (detail of the derivation of the pipe displacement in terms of the Fourier series is provided in appendix A)

$$\begin{aligned}
u(s,\theta,t)&=\frac{1}{2\pi}\int_{-\infty}^{\infty}\sum_{n=0}^{\infty}\varepsilon_n\overline{U_n(k_{nb})}\cos(n\theta)\,e^{j(k_{nb}s-\pi/2-\omega t)}dk_{nb}\\
v(s,\theta,t)&=\frac{1}{2\pi}\int_{-\infty}^{\infty}\sum_{n=0}^{\infty}\varepsilon_n\overline{V_n(k_{nb})}\sin(n\theta)\,e^{j(k_{nb}s-\omega t)}dk_{nb} \qquad \ldots(2.13)\\
w(s,\theta,t)&=\frac{1}{2\pi}\int_{-\infty}^{\infty}\sum_{n=0}^{\infty}\varepsilon_n\overline{W_n(k_{nb})}\cos(n\theta)\,e^{j(k_{nb}s-\omega t)}dk_{nb}
\end{aligned}$$

where $\varepsilon = 1$ for $n = 0$ and

$\varepsilon = 2$ for $n \geq 1$.

Because axial wavenumbers are continuous and the mode number is discrete, the delta functions of $\delta(s)$ and $\delta(\theta - \phi)$ may be expressed as

$$\delta(s) = \frac{1}{2\pi}\int_{-\infty}^{\infty} e^{jk_{nb}s}\,dk_{nb}$$

$$\delta(\theta-\phi) = \frac{1}{2\pi}\sum_{n=-\infty}^{\infty} e^{jn(\theta-\phi)}$$

So, the point force in equation (2.11) in the wavenumber domain can be written as

$$F(s,\theta,t) = \frac{1}{4\pi^2 a^2}\int_{-\infty}^{\infty}\sum_{n=0}^{\infty}\varepsilon_n F_o \cos(n(\theta-\phi))e^{j(k_{nb}s-\omega t)}\,dk_{nb} \qquad \ldots(2.14)$$

By substitution of the displacements and point force into equation (2.12), the spectral response of the pipe to the applied force is given by

$$\begin{bmatrix} L_{11} & L_{12} & L_{13} \\ L_{21} & L_{22} & L_{23} \\ L_{31} & L_{32} & L_{33} \end{bmatrix}\begin{bmatrix} \overline{U_n(k_{nb})} \\ \overline{V_n(k_{nb})} \\ \overline{W_n(k_{nb})} \end{bmatrix} = \begin{bmatrix} 0 \\ 0 \\ -\dfrac{\Omega^2 F_o}{2\pi\omega^2\rho h a^2}\dfrac{\cos(n(\theta-\phi))}{\cos(n\theta)} \end{bmatrix} \qquad \ldots(2.15)$$

By inversion of the 3x3 matrix, the amplitudes of the displacements can be written as

$$\begin{bmatrix} \overline{U_n(k_{nb})} \\ \overline{V_n(k_{nb})} \\ \overline{W_n(k_{nb})} \end{bmatrix} = \begin{bmatrix} I_{11} & I_{12} & I_{13} \\ I_{21} & I_{22} & I_{23} \\ I_{31} & I_{32} & I_{33} \end{bmatrix}\begin{bmatrix} 0 \\ 0 \\ -\dfrac{\Omega^2 F_o}{2\pi\omega^2\rho h a^2}\dfrac{\cos(n(\theta-\phi))}{\cos(n\theta)} \end{bmatrix} \qquad \ldots(2.16)$$

The spectral radial displacement is given by

$$\overline{W_n(k_{nb})} = -\frac{\Omega^2 F_o}{2\pi\omega^2\rho\, h a^2}\frac{\cos(n(\theta-\phi))}{\cos(n\theta)} I_{33} \qquad \ldots(2.17)$$

Omitting terms of $e^{-j\omega t}$ for simplification, the radial displacement for a particular mode in the frequency domain is obtained by substituting equation (2.17) into equation (2.13) as

$$\overline{\overline{W}}_n(s,\theta) = -\frac{\varepsilon_n\Omega^2 F_o[\lambda_1\cos(n\theta)+\lambda_2\sin(n\theta)]}{4\pi^2\omega^2\rho h a^2}\int_{-\infty}^{\infty} I_{33}e^{jk_{nb}s}\,dk_{nb} \qquad \ldots(2.18)$$

where $I_{33} = \dfrac{L_{11}L_{22} - L_{12}L_{21}}{\text{Det}\,|L|}$

$\lambda_1 = \cos(n\phi)$

$\lambda_2 = \sin(n\phi)$

For each frequency, the parameter I_{33} has eight poles, so residue theory is applied to solve the integration. With this method, only the upper half plane of the complex plane is integrated by running above the negative real axis and running below the positive real axis so that only four poles are analysed. Physically, this means that for a semi-infinite pipe only 4 waves can potentially propagate along the pipe. Hence, the solution of equation (2.18) is

$$\overline{\overline{W}}_n(s,\theta) = -\frac{j\varepsilon_n \Omega^2 F_o [\lambda_1 \cos(n\theta) + \lambda_2 \sin(n\theta)]}{2\pi\omega^2 \rho h a^2} \sum_{b=1}^{4} \text{Res}_b e^{jk_{nb}s} \qquad \ldots(2.19)$$

where $\text{Res}_b = \dfrac{L_{11}L_{22} - L_{12}L_{21}}{(\text{Det}\,|L|)'}$

$$(\text{Det}\,|L|)' = \frac{\partial(\text{Det}\,|L|)}{\partial k_{nb}}$$

The mobility of the forced response on the n^{th} mode is given by

$$Y_n = -j\omega \frac{\overline{\overline{W}}_n(s,\theta)}{F_o} = -\frac{\varepsilon_n \Omega^2 [\lambda_1 \cos(n\theta) + \lambda_2 \sin(n\theta)]}{2\pi\omega\rho\, h a^2} \sum_{b=1}^{4} \text{Res}_b e^{jk_{nb}s} \qquad \ldots(2.20)$$

The $\text{Det}\,|L|$ is given by equation (2.8) and its derivative with respect to k_{nb} is given by

$$\frac{\partial(\text{Det}\,|L|)}{\partial k_{nb}} = 2(1-\nu)k_{ab}\left[2\beta^2(k_{nb}^2 + n^2)(k_{nb}^2 + n^2 - 1)(k_{nb}^2 + n^2 - \frac{1}{2}) + (1-\nu^2)k_{nb}^4 - \Omega^2(k_{nb}^2 + n^2 + \frac{1}{2})\right] \qquad \ldots(2.21)$$

The term $(L_{11}L_{22} - L_{12}L_{21})$ is given by

$$L_{11}L_{22} - L_{12}L_{21} = \frac{1}{2}(1-\nu)(k_{nb}^2 + n^2)^2 - \frac{1}{2}(3-\nu)(k_{nb}^2 + n^2)\Omega^2 + \frac{1}{4}\beta^2\left[(1-\nu)k_{nb}^2(k_{nb}^2 + n^2) - \frac{5}{2}k_{nb}^2 n^2\right] \qquad \ldots(2.22)$$

Using the previous assumptions of $\beta^2 << 1$ and $k_{nb}^2 >> \Omega^2$, then the second and the last term can be neglected and equation (2.22) becomes

2.7 Experimental Results

In this section, several experimental results are presented and where applicable predictions calculated using the theory described in the previous section are overlaid.

The prediction of the accelerance of the pipe for a particular mode provided in equation (2.25) was verified by the modal amplitude extracted from the experimental results by the modal decomposition method, which is described in appendix C. It was also compared with the experiment results when the mass effect of an accelerometer, which is described in appendix D, is taken account. In addition, the orientation angle, ϕ, with respect to the point force position is also described in this appendix. Once the orientation is determined, the total accelerance of the pipe can be calculated by summing equation (2.25) for all modes as

$$H = \sum_{n=0}^{\infty} \frac{j\varepsilon_n \Omega^2 [\lambda_1 \cos(n\theta) + \lambda_2 \sin(n\theta)]}{2\pi\rho h a^2} \sum_{b=1}^{4} \mathrm{Re}\, s_b e^{jk_{nb}s} \qquad \ldots(2.26)$$

Because the mass of the accelerometer has an effect on the response of the pipe at high frequencies, the mass of the accelerometer has to be taken account and the procedure to do this is described in appendix D.

The experimental results presented are as follows.

Mode Decomposition from Measured Results at Distance 300 mm from the Excitation Point

Figure 2.7: Mode decomposition of n = 0 mode
Figure 2.8: Mode decomposition of n = 1 mode
Figure 2.9: Mode decomposition of n = 2 mode
Figure 2.10: Mode decomposition of n = 3 mode
Figure 2.11: Orientation angle obtained at n = 1 mode
Figure 2.12: Orientation angle obtained at n = 2 mode
Figure 2.13: Orientation angle obtained at n = 3 mode

Frequency Response at a Distance 300 mm from the Excitation Point

$$L_{11}L_{22} - L_{12}L_{21} = \frac{1}{2}(1-\nu)(k_{nb}^2 + n^2)^2 \qquad \ldots(2.23)$$

So, the residue term is

$$Res_b = \frac{(k_{nb}^2 + n^2)^2}{4\,k_{ab}\left[2\beta^2(k_{nb}^2 + n^2)(k_{nb}^2 + n^2 - 1)(k_{nb}^2 + n^2 - \frac{1}{2}) + (1-\nu^2)k_{nb}^4 - \Omega^2(k_{nb}^2 + n^2 + \frac{1}{2})\right]} \qquad \ldots(2.24)$$

The accelerance of the n^{th} mode is given as

$$\begin{aligned} H_n &= -j\omega Y_n \\ &= \frac{j\varepsilon_n \Omega^2 [\lambda_1 \cos(n\theta) + \lambda_2 \sin(n\theta)]}{2\pi\rho\, ha^2} \sum_{b=1}^{4} Res_b e^{jk_{nb}s} \end{aligned} \qquad \ldots(2.25)$$

2.5 Numerical analysis of point force mobility

In the previous section it was shown that Flugge and Kennard shell theories provided consistent predictions of the cut-on frequencies and of the wavenumber and compared well with simplified equations derived. In this section, a numerical comparison between them is carried out using the point force mobility. Due to the limitation of the computer, the frequency response of the total mobility, $Y = \sum_{n=0}^{\infty} Y_n$ is truncated at n = 7. Using the pipe data from Table 2.1, the plot of $Y(s=0, \theta=0)$ against frequency is shown in figure 2.5.

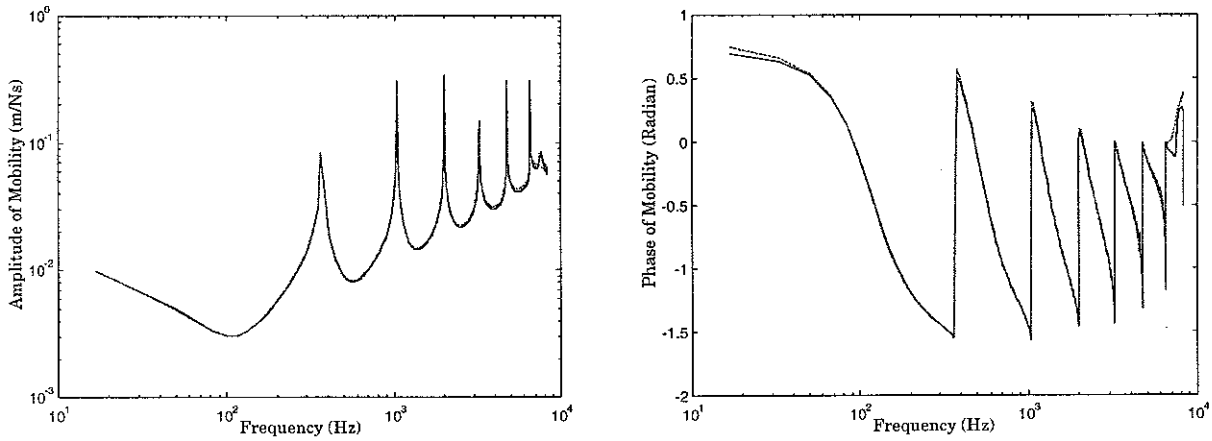

Figure 2.5. Amplitude and phase of point mobility with ϕ = 0; ···, Flugge's version; —, Kennard's version; ---, equation (2.20).

The above results show the consistency of the point mobility calculated using three expressions, and also the consistency of the cut-on frequency obtained using these expressions. The disagreements that occur at high frequencies are due to the different assumptions.

2.6 Experimental Setup and Procedure

Since several approximations are involved in the derivation of the equations in this work, it is useful to validate them by experiments. In this section, the experiments that were carried out to verify the simplified version of shell theory are described. Before the experiment on the pipe was conducted, the sensitivity of the piezoelectric element attached to the tip of small shaker in order to measure an input force had to be determined. The sensitivity of the piezoelectric element in terms of charge per Newton was calibrated using a known mass of 4.384 kg.

Since the pipe discussed in the previous section was assumed to be semi-infinite, which has no reflected waves from one end of the pipe, an anechoic termination was used for this purpose. However, this does not perfectly absorb vibration so that some reflection from the anechoic termination still remains which interferes with the incident waves. It is useful to evaluate the effectiveness of the termination in terms of the ratio of incident to reflected waves from the experimental results. To separate both incident and reflected waves, the method of wave decomposition described in appendix B was applied.

The experimental setup for the wave decomposition and for verification of the simplified version of the shell theory is shown in figure 2.6. A 2.7 m plastic pipe was suspended by cords and was free at one end and had an anechoic termination at the other end. The pipe was excited at the free end by the small shaker. A random signal was supplied to the shaker from an HP 3566A Signal Analyzer and three sets of frequency response functions of the pipe were measured using Bruel & Kjaer accelerometers type 4375, located at a distance of 300, 1500 and 1550 mm from the shaker. The thirty-two measurements around the circumference of the pipe were conducted at each axial position and the frequency response functions of the pipe in terms of accelerance were analysed using the Signal Analyzer. The two sets of measurements at axial positions

1500 and 1550 mm, which are in the far field from the source, were used to decompose the incident and reflected waves. Another set of measurements was taken at the location of 300 mm, which is in the near field of the source. The results from this measurement position are used to verify the simplified version of the shell theory developed in the previous section. The reason for selecting the measurement position in the near field was to capture the direct waves generated by the shaker (flexural, near field and standing near field waves) so that they are not distorted by the reflected waves. Since two accelerometers were used for wave decomposition, phase matching and cross sensitivity between them had to be determined prior to applying such a technique to avoid ill-conditioning.

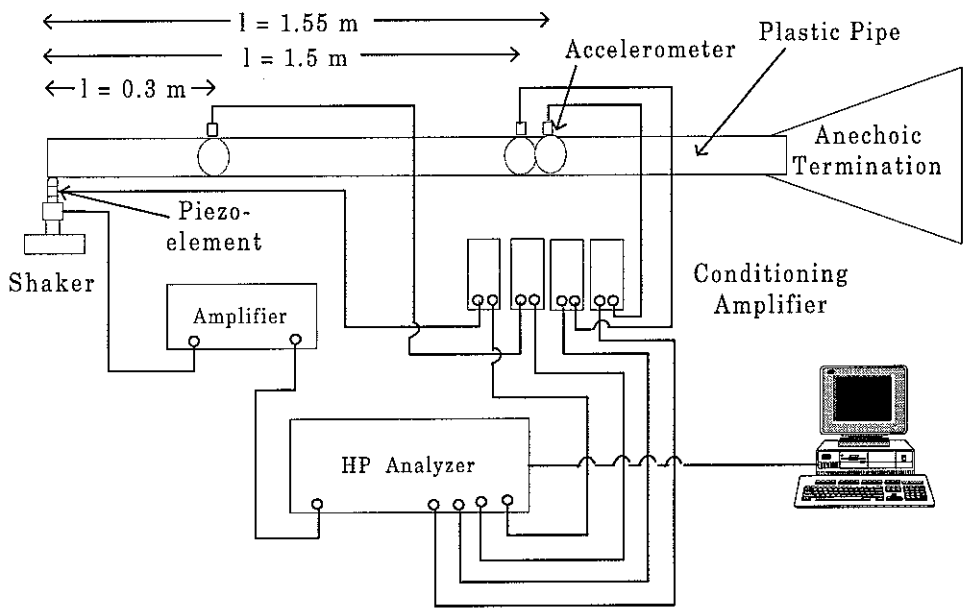

Figure 2.6: Experimental setup for the mode and for the wave decompositions

Figure 2.14: Accelerance of the pipe at $\theta = 0$ and $\phi = 13$

Wave Decomposition from Measured Results at Distance 1500 mm and 1550 mm from Excitation Point

Figure 2.15: Wave ratio of incident to reflected waves of n = 0 mode

Figure 2.16: Wave ratio of incident to reflected waves of n = 1 mode

Figure 2.17: Wave ratio of incident to reflected waves of n = 2 mode

Figure 2.18: Wave ratio of incident to reflected waves of n = 3 mode

Figure 2.19: Wave ratio of total incident to total reflected waves

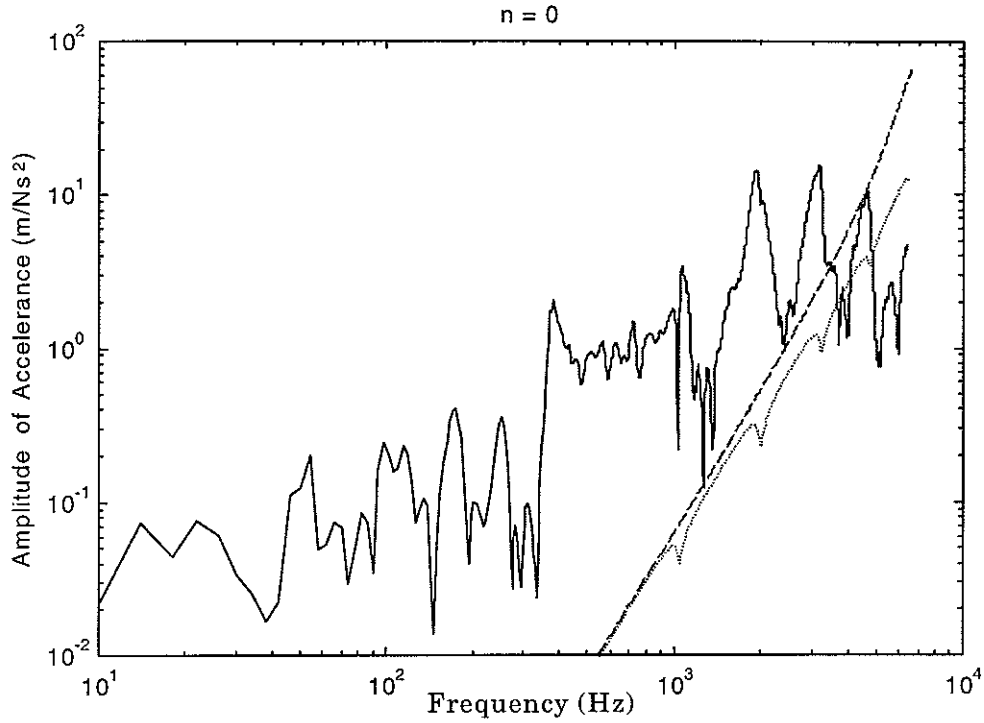

Figure 2.7: Decomposition of n = 0 mode: —Measured result; --- equation (2.25); ... equation (2.25) with mass effect accounted for.

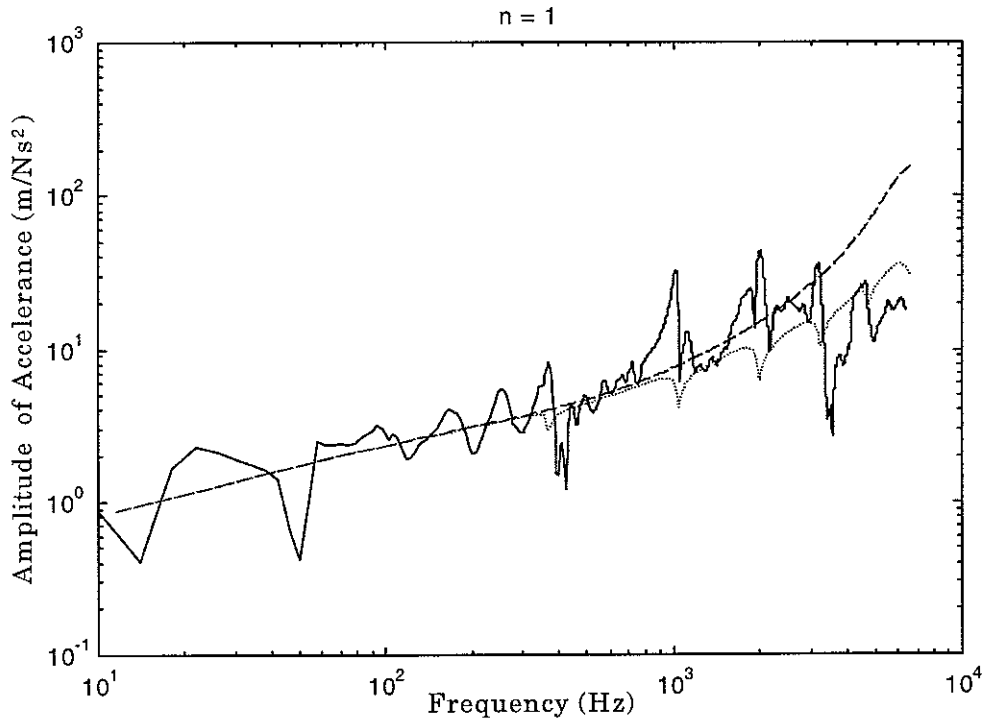

Figure 2.8: Decomposition of n = 1 mode: — Measured result; --- equation (2.25); ... equation (2.25) with mass effect accounted for.

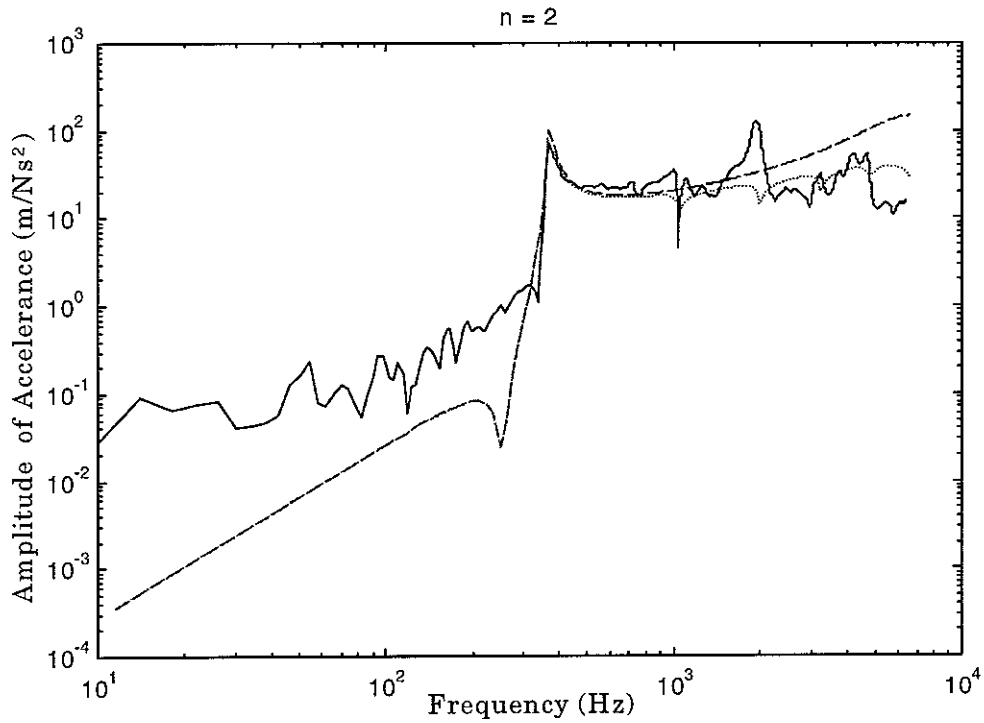

Figure 2.9: Decomposition of n = 2 mode: — Measured result; --- equation (2.25); ... equation (2.25) with mass effect accounted for.

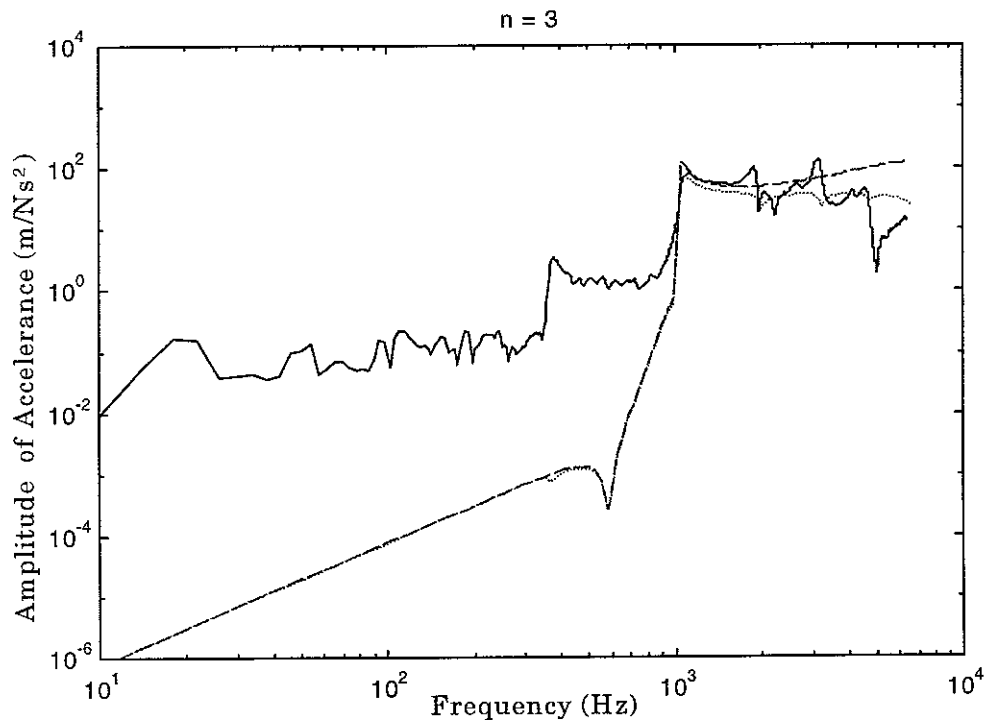

Figure 2.10: Decomposition of n = 3 mode:—Measured result; --- equation (2.25); ... equation (2.25) with mass effect accounted for.

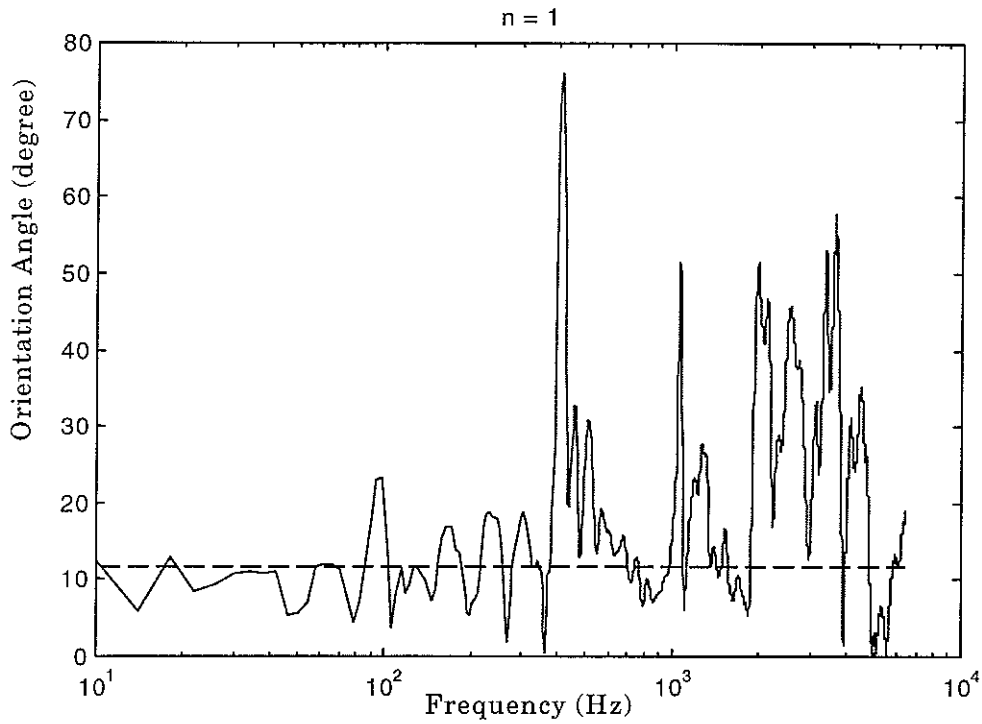

Figure 2.11: Orientation angle of the pipe with respect to the force position extracted at n = 1 mode; --- 13^0.

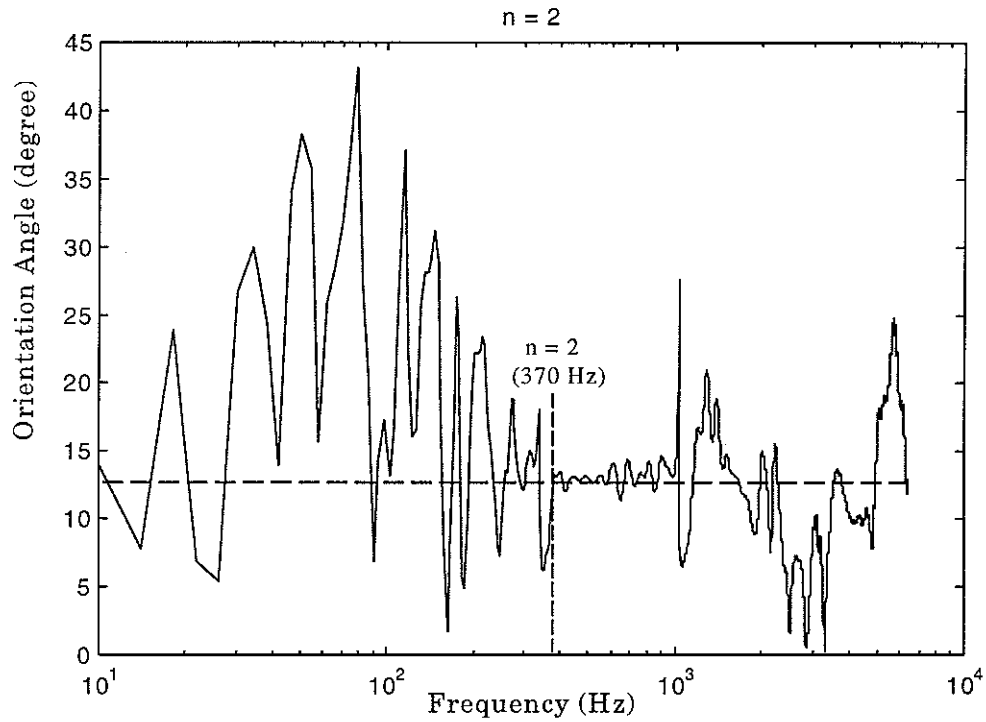

Figure 2.12: Orientation angle of the pipe with respect to the force position extracted at n = 2 mode; --- 13^0.

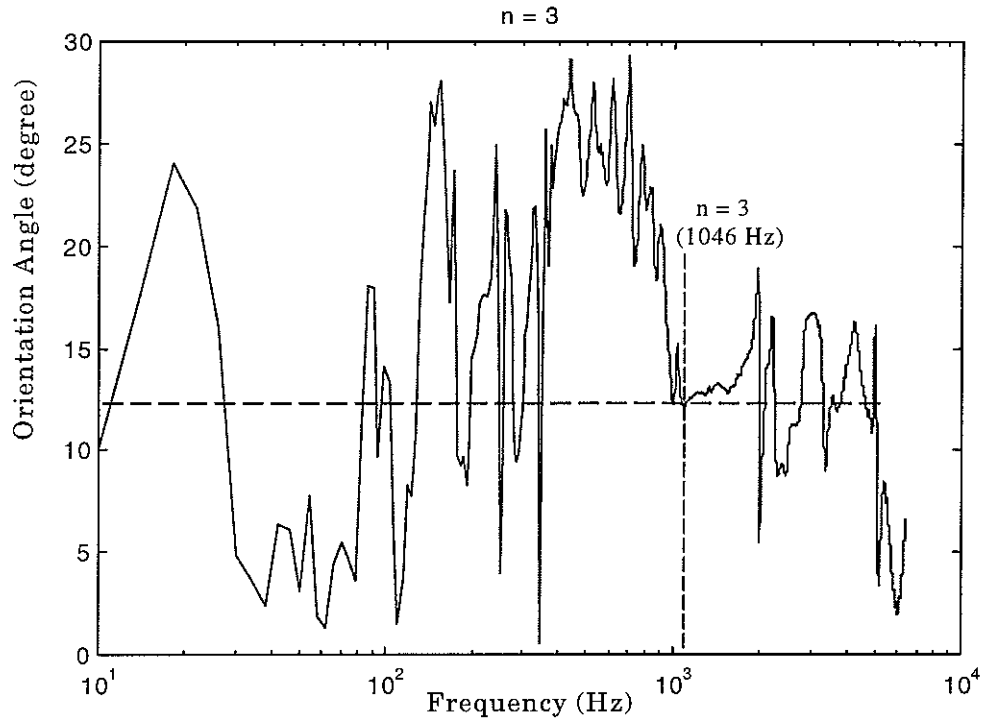

Figure 2.13: Orientation angle of the pipe with respect to the force position extracted at n = 3 mode; --- 12^0.

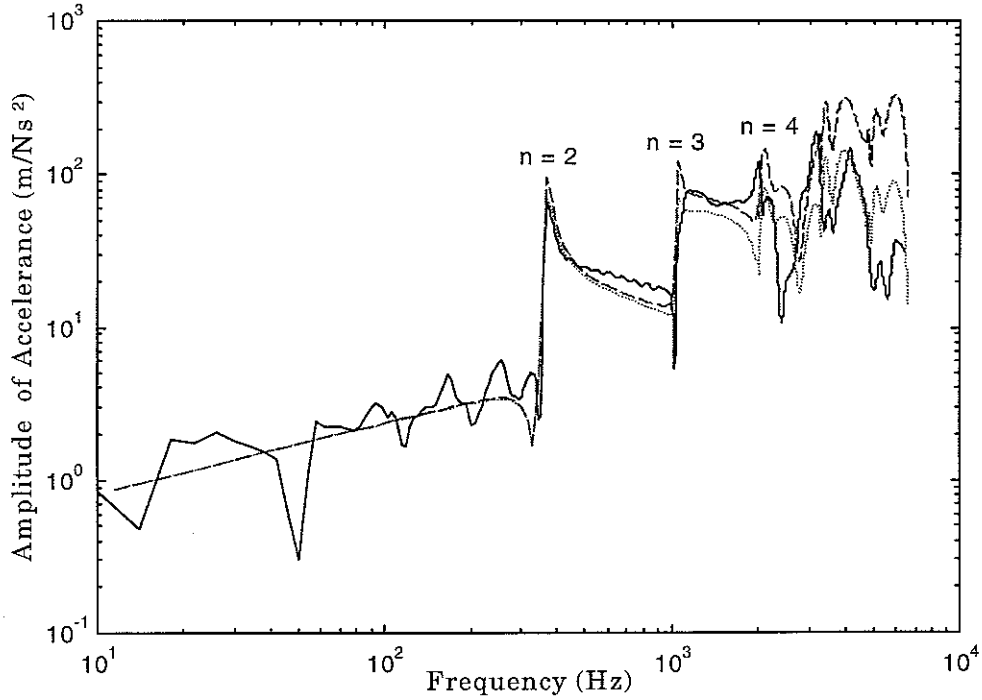

Figure 2.14: Accelerance of the pipe with $\theta = 0$ and $\phi = 13$:—— Measured result; --- equation (2.26); ... equation (2.26) with mass effect accounted for.

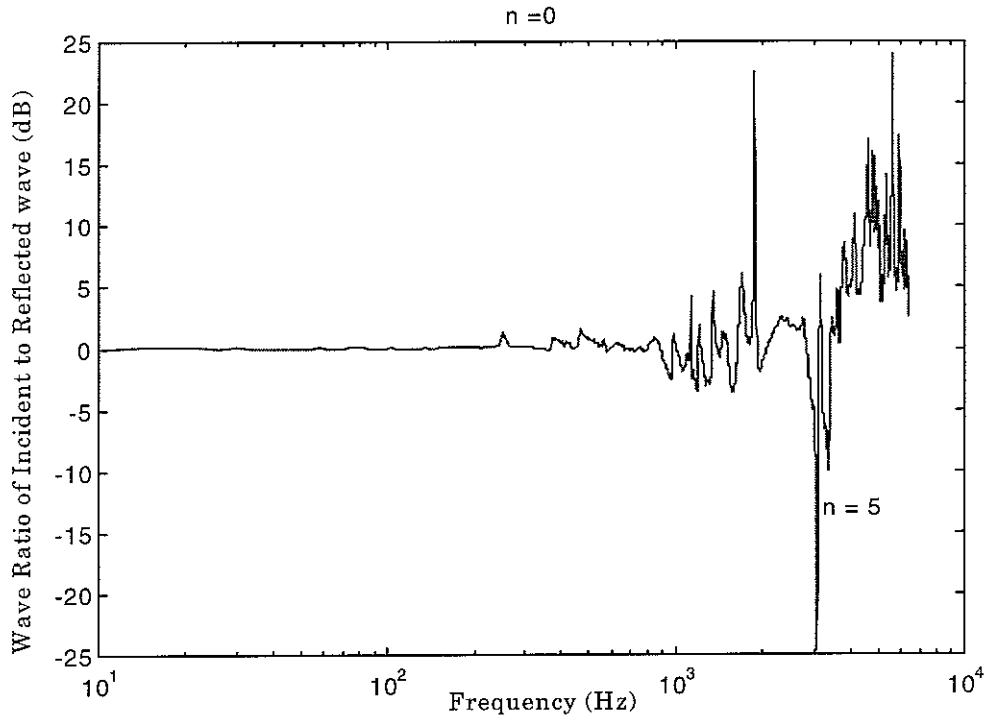

Figure 2.15: Wave ratio of Incident to reflected waves of n = 0 mode

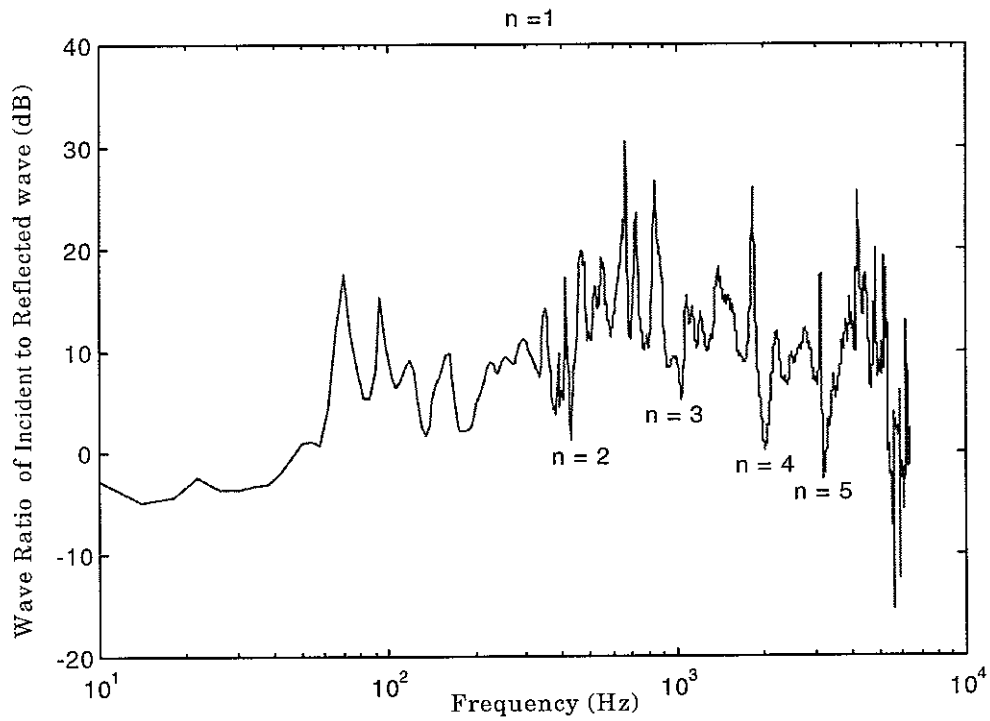

Figure 2.16 : Wave ratio of Incident to reflected waves of n = 1 mode

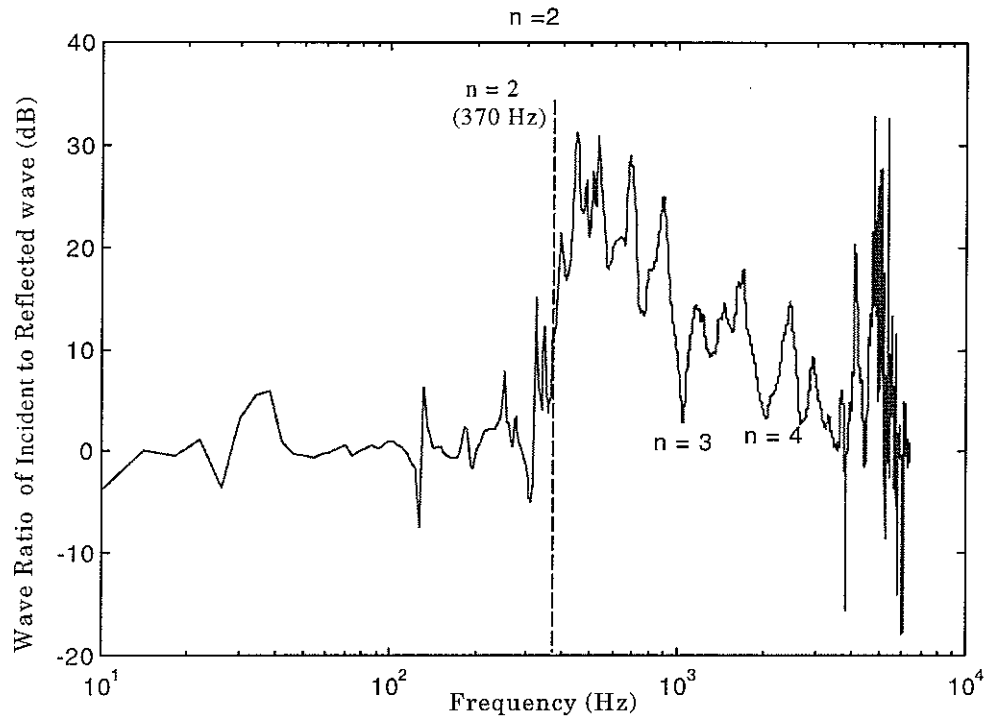

Figure 2.17: Wave ratio of Incident to reflected waves of n = 2 mode

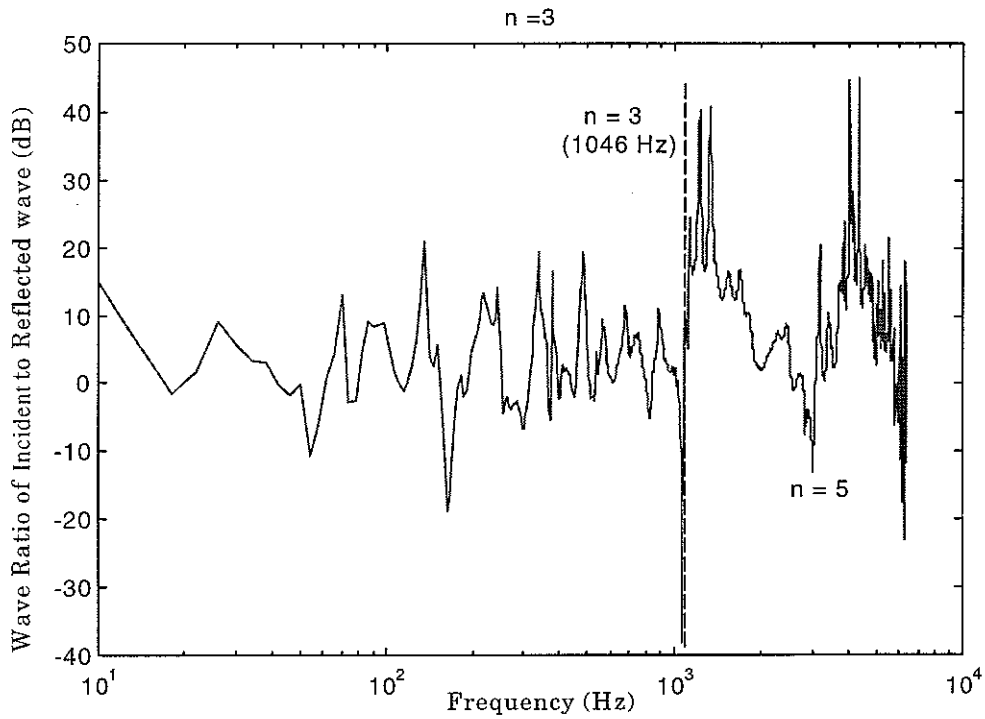

Figure 2.18: Wave ratio of Incident to reflected waves of n = 3 mode

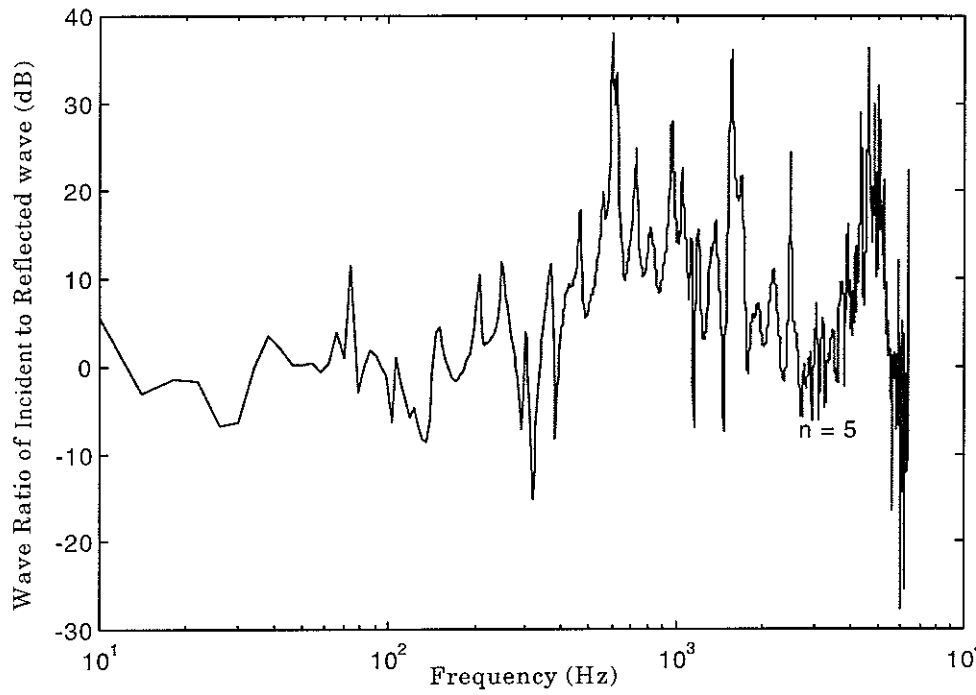

Figure 2.19: Wave ratio of total Incident to reflected waves.

2.8 Discussion

From figures 2.7-2.10 and figure 2.14, it is clear that even if the mass of the accelerometer is small (2.4 grams), it still has a large effect on the motion of the pipe at high frequencies. This is because the mobility of the pipe is high at high frequencies, while the mobility of the accelerometer is low at high frequencies ($1/jm\omega$) causing a reduction of pipe velocity at the measurement position in the high frequency region. It is also shown in figure 2.7, 2.9 and 2.10 that, before the waves cut on, the motion of the pipe for particular mode is very small. It is difficult to obtain these modal amplitudes by the modal decomposition technique because of the requirement to accurately position of sensors in order to cancel out the response from undesired modes and due to noise in the measured results. Because of the finite length of the pipe, it possibly behaves like a mass at low frequencies which results in a motion that is higher than that predicted using the theoretical model. Such a difference does not occur for the motion of the $n = 1$ mode shown in figure 2.8 because its dynamic behaviour is already rigid body in the radial direction. To calculate the motion of the pipe with and without the effect of the accelerometer mass, its orientation with respect to the force position must firstly be obtained. This is approximately 13 degrees, which is shown in figures 2.11 – 2.13. It should be noted that the orientation angle was determined after the structural waves had cut on because of the mass-like behaviour and poor signal to noise ratio at the low frequencies.

From figures 2.15 – 2.18, it can be seen that the anechoic termination adequately suppressed the flexural waves but was not very effective in suppressing the longitudinal wave. To suppress the longitudinal wave, another kind of termination should be applied such as a plate of an appropriate impedance (Brennan et al [16]). Some suppression of the flexural wave was obtained after the waves had cut on and it degrades when other modes, which are reflected at the discontinuity (anechoic termination), cut on.

3. Modal Sensors

3.1 Introduction

Both the mass effect and the number of point measurements required for modal decomposition are disadvantages of using an accelerometer to sense the motion of a pipe. It is expected that a polyvinylidene fluoride (PVDF) sensor will overcome some of these problems. Since PVDF is lightweight, it will not change the mechanical property of the pipe. Because it has a distributed surface for sensing the motion of the pipe and can be cut into the shapes of sine and cosine functions, it can measure the response of a particular mode without any processing of the measurements.

In this chapter, the theory for a modal sensor for a circumferential mode of a pipe, especially the n = 2 mode, is developed. Some experiments are carried out to verify this theory. In addition, the performance of the modal sensor and of the accelerometer is compared in the form of accelerance. The comparison is taken to see the mass effect of both sensors in order to select a proper sensor for a pipe in an active vibration control system.

3.2 Modal sensor for pipe

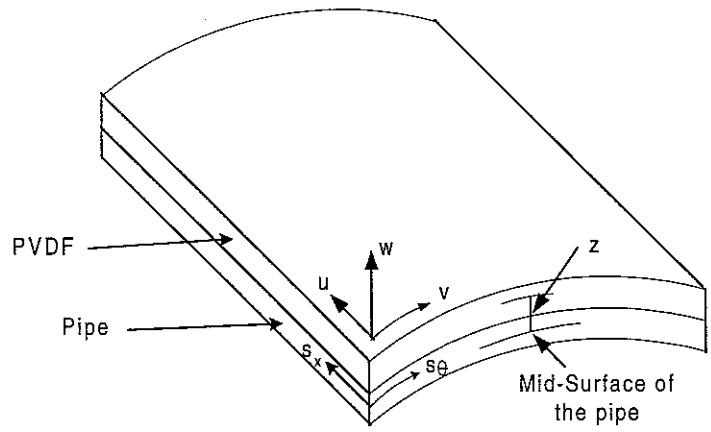

Figure 3.1: Schematic of composite section of a pipe

A schematic of a composite section of a pipe, which consists of an inner layer of pipe and an outer layer of sensor, is shown in figure 3.1. Generally, the mid-surface of the pipe itself is changed due to increasing thickness, however since the distributed PVDF sensor is very thin, it is assumed that the mid-surface of the pipe is unchanged. The assumption, that the sensor is completely bonded on the pipe, is also made so that the strain is continuously distributed through the composite pipe. It is well known that to be a sensor the PVDF uses the direct piezoelectric effect, which converts mechanical strain to an electrical charge (Lee [17]). Without a skew angle, which is the angle between axes of the sensor and of the pipe, this phenomenon may be represented (Lee [17] and Lee and Moon [8]) as

$$D_3 = \varepsilon_{33}E_3 + e_{31}S_\theta + e_{32}S_x \qquad \ldots(3.1)$$

where

D_3 is the electric displacement (C/m^2),

S_x and S_θ are the axial and circumferential strains (m/m), respectively,

ε_{33} is the permittivity at constant stress (F/m),

E_3 is the electric field (V/m),

e_{31} and e_{32} are the piezoelectric stress constants (C/m^2).

The piezoelectric strain constants can be determined from

$$\begin{bmatrix} e_{31} \\ e_{32} \end{bmatrix} = \begin{bmatrix} E_{pv}/(1-\nu_{pv}^2) & \nu_{pv}E_{pv}/(1-\nu_{pv}^2) \\ \nu_{pv}E_{pv}/(1-\nu_{pv}^2) & E_{pv}/(1-\nu_{pv}^2) \end{bmatrix} \begin{bmatrix} d_{31} \\ d_{32} \end{bmatrix} \qquad \ldots(3.2)$$

where

E_{pv} is Young's modulus of PVDF (N/m^2),

ν_{pv} is Poisson's ratio of PVDF (no unit),

d_{31} and d_{32} are the piezoelectric strain constants (C/N).

Following Flugge's shell theory (Liessa [1], Flugge [18]), the axial (S_x) and circumferential (S_θ) strains at arbitrary distance z from the mid-surface of a pipe may be expressed in terms of the pipe strain combination between stretching (extensional deformation) and bending (in-extensional deformation) strains of the mid-surface of the pipe as

$$S_x = S_{ex} + S_{ix} \quad \text{and}$$

$$S_\theta = \frac{1}{1+z/a}(S_{e\theta} + S_{i\theta}) \qquad \ldots(3.3\ a,b)$$

where a is the radius of the pipe,

$S_{ex} = \frac{\partial u}{\partial x}$ is the longitudinal or stretching strain in axial direction,

$S_{ix} = -z\frac{\partial^2 w}{\partial x^2}$ is the bending strain in axial direction,

$S_{e\theta} = \frac{1}{a}\left(\frac{\partial v}{\partial \theta} + w\right)$ is the stretching strain in circumferential direction and

$S_{i\theta} = -\frac{z}{a^2}\left(\frac{\partial^2 w}{\partial \theta^2} - \frac{\partial v}{\partial \theta}\right)$ is the bending strain in circumferential direction.

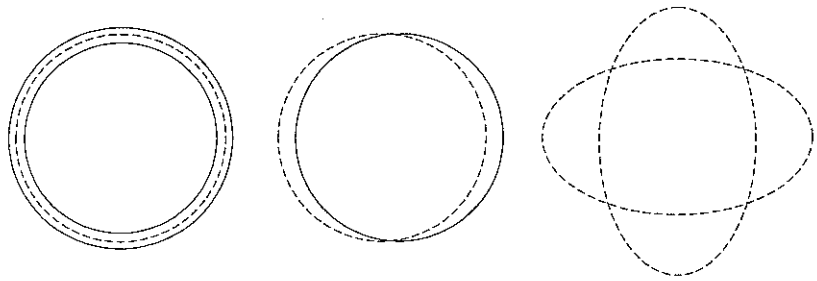

Figure 3.2: Forms of mode deformation of a pipe.

It is well known that the extensional deformation dominates the motion of the pipe for the n = 0 mode, while the deformation of n = 1 or higher modes is in-extensional (Flugge [18] and Timoshenko and Woinowsky-Krieger [19]). Since the main aim of this work is to develop the modal sensor of the n = 2 mode of the pipe, in which the stretching strains (S_{ex} and $S_{e\theta}$) equal to zero, only the bending strains (S_{ix} and $S_{i\theta}$) represent the motion of the pipe. One of the conditions for in-extensional deformation (Timoshenko and Woinowsky-Krieger [19]) is $\frac{\partial v}{\partial \theta} = -w$, then $S_{i\theta} = -\frac{z}{a^2}\left(\frac{\partial^2 w}{\partial \theta^2} + w\right)$. For simplification, the term z/a may also be neglected in comparison with unity so that equation (3.3) becomes

$$S_x = -z\frac{\partial^2 w}{\partial x^2} \text{ and}$$

$$S_\theta = -\frac{z}{a^2}\left(\frac{\partial^2 w}{\partial \theta^2} + w\right) \quad \text{for } n \geq 1 \qquad \ldots(3.4\text{ a, b})$$

In the case that the width of the sensor is much smaller than the wavelength of a propagating wave, the axial strain is approximately constant over the width of the sensor. The assumption will be justified later in terms of the maximum width of the sensor. Assuming the strains discussed above, the electric displacement given in equation (3.1) becomes

$$D_3 = \varepsilon_{33}E_3 - e_{31}\frac{z}{a^2}\left(\frac{\partial^2 w}{\partial \theta^2} + w\right) + e_{32}S_x \qquad \ldots(3.5)$$

In order to measure the charge generated from the PVDF sensor, a closed-circuit arrangement (Lee [17] and Callahan and Baruh [13]), in which the surface electrodes of both sides of the sensor are short-circuited, is employed so that the electric field E_3 is zero. By such an arrangement, the generated charge is approximately the average of the electric displacement integrated over the area of both sides of the effective surface electrodes. So

$$q(t) = \frac{1}{2}\left(\iint_{A_p(z=z_o+h_{pv}/2)} D_3 a\,dx\,d\theta + \iint_{A_p(z=z_o-h_{pv}/2)} D_3 a\,dx\,d\theta\right) \qquad \ldots(3.6)$$

where A_p is the effective surface area of the PVDF,

h_{pv} is the thickness of the PVDF,

$z_o = (h + h_{pv})/2$ is the distance from the mid-plane of the pipe to that of the PVDF,

h is the thickness of the pipe and

a is the radius of the pipe.

Substituting the electric displacement from equation (3.5) into equation (3.6), it becomes

$$q(t) = \iint_{A_p}\left[-z_o e_{31}\left(\frac{\partial^2 w}{\partial \theta^2} + w\right) + a^2 e_{32}S_x\right] ds\,d\theta \qquad \ldots(3.7)$$

where s = x/a is the non-dimensional longitudinal distance.

The radial shell displacement for a semi-infinite pipe has already been discussed in the previous chapter (equation 2.2) and is given here for clarity

$$w(s,\theta,t)=\sum_{n=1}^{\infty}\sum_{b=1}^{4}W_n\left(\lambda_1\cos(n\theta)+\lambda_2\sin(n\theta)\right)e^{j(k_{nb}s-\omega t)} \qquad ...(3.8)$$

where $\lambda_1 = \cos(n\phi)$,

$\lambda_2 = \sin(n\phi)$ and

ϕ is the orientation angle.

It should be noted that the displacement of the n = 0 mode is not included in above expression since the extensional deformation is not taken into account in this work.

Substituting the displacement of equation (3.8) into equation (3.7) gives

$$q(t)=\sum_{n=1}^{\infty}\sum_{b=1}^{4}A_nW_n\int_{A_p}\left(\lambda_1\cos(n\theta)+\lambda_2\sin(n\theta)\right)e^{j(k_{nb}s-\omega t)}dsd\theta+a^2\int_{A_p}e_{32}S_x\,dsd\theta \qquad ...(3.9)$$

where

$$A_n=z_oe_{31}\left(n^2-1\right)$$

Since the total charge generated, q(t), is the sum of the response over the surface of the PVDF sensor, it may be expressed as (Gu et al [9])

$$q(t)=\sum_{n=1}^{\infty}\sum_{b=1}^{4}A_nW_n\int_0^{2\pi}\int_{s_c-b_sS_p(\theta)}^{s_c+b_sS_p(\theta)}\left(\lambda_1\cos(n\theta)+\lambda_2\sin(n\theta)\right)e^{j(k_{nb}s-\omega t)}dsd\theta+a^2\int_0^{2\pi}\int_{s_c-b_sS_p(\theta)}^{s_c+b_sS_p(\theta)}e_{32}S_x\,dsd\theta$$

... (3.10)

where s_c is the non-dimensional axial location of centre of the sensor to the radius of the pipe,

b_s is the ratio of a half of width of the sensor to the radius of the pipe,

$S_p(\theta)$ is the shape of the sensor.

Evaluating the integral, we get (omitting the terms of $e^{-j\omega t}$ for simplification)

$$q = \sum_{n=1}^{\infty}\sum_{b=1}^{4}\frac{2e^{jk_{nb}s_c}}{k_{nb}}A_n W_n \int_0^{2\pi}\{\lambda_1 \cos(n\theta)+\lambda_2 \sin(n\theta)\}\sin\{k_{nb} b_s S_p(\theta)\}d\theta + 2a^2 b_s e_{32} S_x \int_0^{2\pi} S_p(\theta)d\theta \quad \ldots (3.11)$$

If the sensor is shaped in the form of $S_p(\theta) = \cos(p\theta)$, where p is the desired mode, then integrating the second term of equation (3.11) over the circumference of the pipe is equal to zero:

$$2a^2 b_s e_{32} S_x \int_0^{2\pi} \cos(p\theta)\, d\theta = 0$$

The schematic explanation of the cancellation of the axial strain for the n = 2 modal sensor is shown in figure 3.3. It illustrates that the summation of generated charge due to axial strain over the surface of the modal sensor is equal to zero. This means the modal sensor for the pipe is insensitive to the axial strain and only detects the circumferential strain.

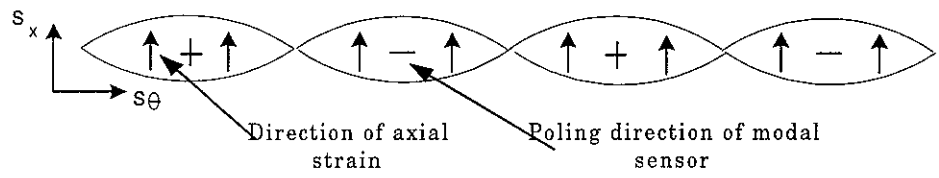

Figure 3.3: Axial strain and Poling directions of a modal sensor for the n = 2 mode

Therefore, equation (3.11) becomes

$$q_c = \sum_{n=1}^{\infty}\sum_{b=1}^{4}\frac{2e^{jk_{nb}s_c}}{k_{nb}}A_n W_n \int_0^{2\pi}\{\lambda_1 \cos(n\theta)+\lambda_2 \sin(n\theta)\}\sin\{k_{nb} b_s \cos(p\theta)\}d\theta \quad \ldots (3.12)$$

Since $\sin\{k_{nb}b_s\cos(p\theta)\}$ can be expressed in terms of Bessel functions as follows (Arfken [20])

$$\sin\{k_{nb} b_s \cos(p\theta)\} = 2\sum_{m=1}^{\infty}(-1)^{m-1} J_{2m-1}(k_{nb} b_s)\cos[(2m-1)p\theta]$$

by substituting it into equation (3.12), using the property of orthogonality gives

$$q_c = \sum_{n=1}^{\infty}\sum_{b=1}^{4}\frac{1}{k_{nb}} 4\pi\lambda_1 e^{jk_{nb}s_c} A_n W_n \sum_{m=1}^{\infty}(-1)^{m-1} J_{2m-1}(k_{nb}b_s)\delta_{nm_p} \qquad \ldots (3.13)$$

where $m_p = (2m\text{-}1)p$.

$\delta_{nm_p} = 1$; for $n = m_p$ and

$= 0$; for $n \neq m_p$.

Equation (3.13) is a general expression for the total charge generated by the modal sensor for any modes with the form of the cosine function. It is clear that the sensor picks up a series of mode displacements. In a specific case of this work, in which p = 2, then the modal sensor will detect the displacements of modes of n = 2, 6, 10 and so on, which correspond to the Bessel function of order 1,3,5 and so on, respectively. Since the interesting frequency range is below the ring frequency, in which the maximum mode is n = 7 ($n_r \cong \sqrt{12}$ a/h; Fahy [14]), the total charge is

$$q_c = 4\pi\lambda_1\left(A_2\sum_{b=1}^{4}\frac{1}{k_{2b}} W_2 J_1(k_{2b}b_s)e^{jk_{2b}s_c} - A_6\sum_{b=1}^{4}\frac{1}{k_{6b}} W_6 J_3(k_{6b}b_s)e^{jk_{6b}s_c}\right) \qquad \ldots(3.14)$$

Because the responses of the n = 2 and n = 6 modes depend upon b_s, the ratio of a half of width of the sensor to the radius of the pipe, therefore, it is interesting to evaluate the cross sensitivity, which is the response of n = 6 mode to that of n = 2 mode, for various b_s. Using the pipe data given from Table 2.1, numerical assessments of the cross sensitivity in near and far fields are shown in figure 3.4. As expected, the cross sensitivity in the near field shown in figure 3.4 largely reduces at 370 Hz where the waves of the n = 2 mode cut on. This does not occur in the far field because there is no motion of the n = 6 mode before it cuts on. Figure 3.4.b clearly shows that the cross sensitivity increases with increasing b_s. Using a criteria of –20 dB cross sensitivity, it illustrates in figure 3.4.c and 3.4.d that, with b_s up to 0.4 in the near field of the vibration source and to 0.2 at the far field, the responses of the n = 6 modes are insignificant. So, equation (3.14) can be reduced to the first term, which is the response of the n = 2 mode. Therefore, the expression of the generated charge becomes

$$q_c = 4\pi\lambda_1 A_2 \sum_{b=1}^{4} \frac{1}{k_{2b}} W_2 J_1(k_{2b} b_s) e^{jk_{2b}s_c} \quad \text{for } n = 2 \text{ and } b_s \le 0.2 \qquad \ldots(3.15)$$

The Bessel function can be expanded as (Arfken [20])

$$J_1(k_{2b} b_s) = \frac{k_{2b} b_s}{2} - \frac{(k_{2b} b_s)^3}{2^3 2!} + \frac{(k_{2b} b_s)^5}{2^5 2!3!} - \ldots$$

where ! is the factorial.

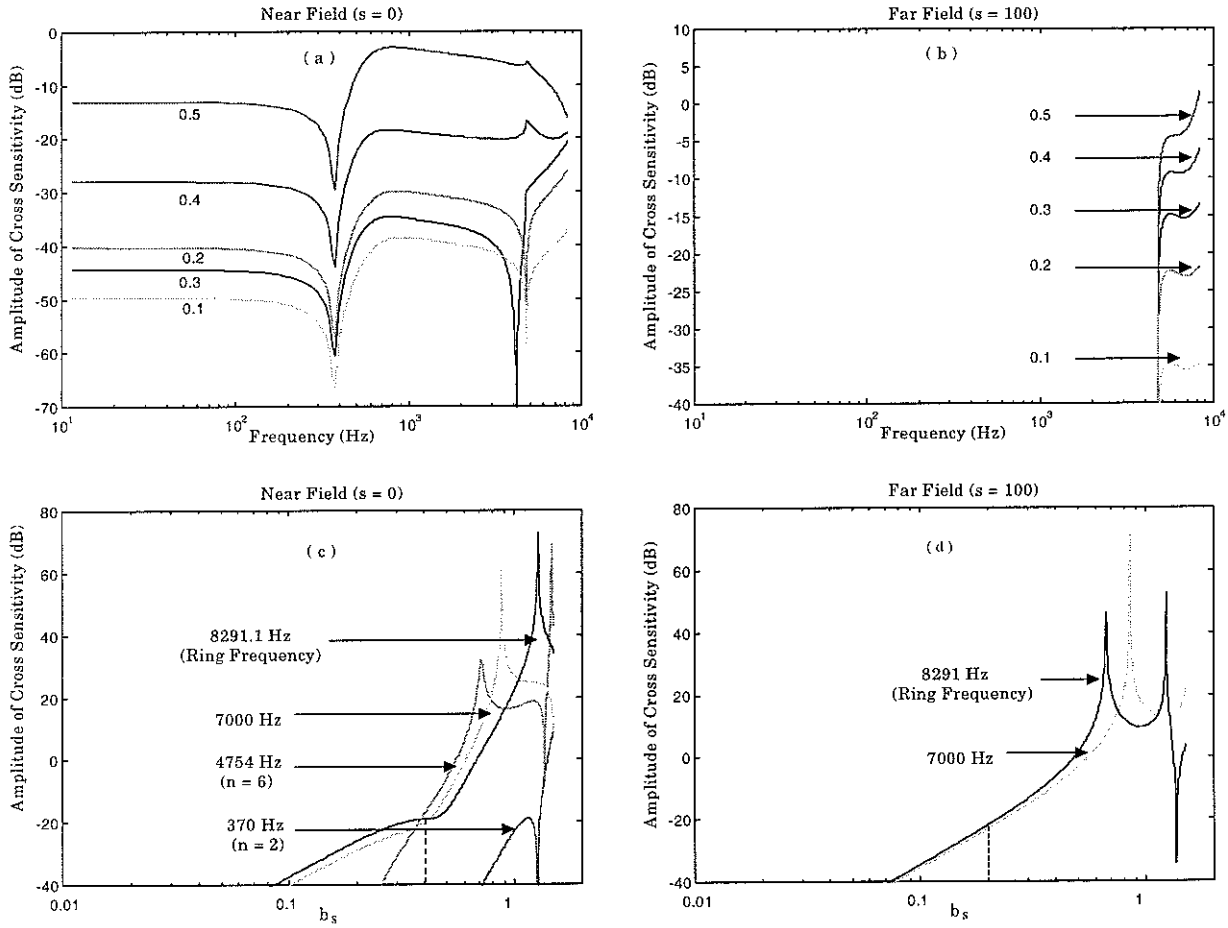

Figure 3.4:Cross sensitivities of the responses of the n = 6 mode to those of the n = 2 mode for various b_s (in (c) and (d), the frequency at 7000 Hz is chosen only to show a trend of the response).

If the product of $k_{2b}b_s$ is less than unity, then higher orders can be ignored. Having the maximum wavenumber of the n = 2 mode at the ring frequency shown in figure 3.5 equal to

approximately 6, b_s should be less than 0.16 to satisfy the above requirement. Hence, the generated charge becomes

$$q_c = 2\pi\lambda_1 b_s A_2 \sum_{b=1}^{4} W_2 e^{jk_{2b}s_c}$$

$$= 2\pi\lambda_1 b_s z_o e_{31}(n^2-1)\sum_{b=1}^{4} W_2 e^{jk_{2b}s_c} \qquad \text{for } n = 2 \text{ and } b_s \le 0.16 \qquad \ldots(3.16)$$

Since the maximum b_s above is less than that obtained from the numerical assessment shown in figure 3.4, it can be used to be the criteria for determination of the ratio of a half of width of the sensor to the radius of the pipe and is

$b_s < 1/k_{2b}$ at the ring frequency.

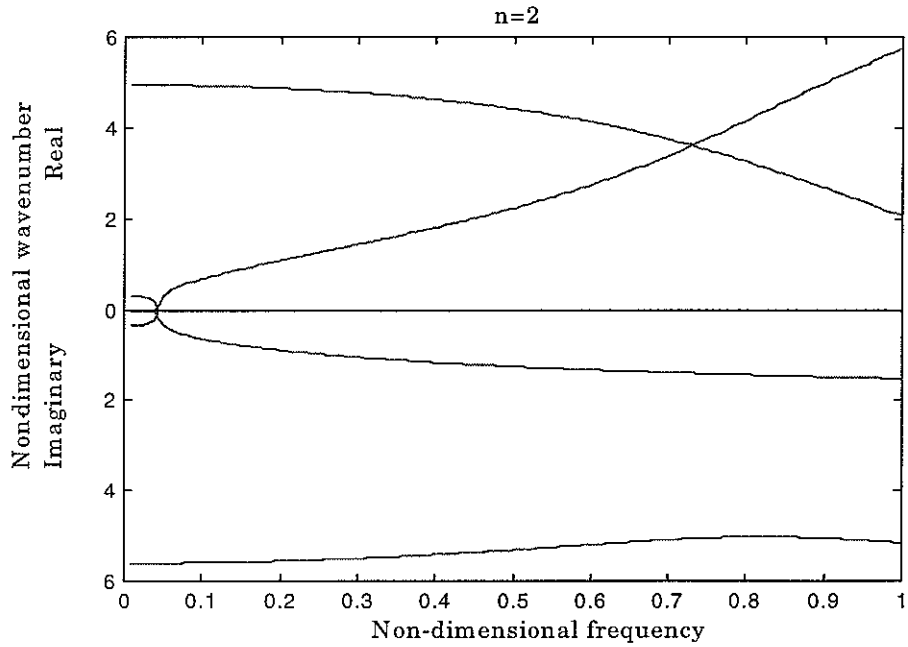

Figure 3.5: Dispersion curve of n = 2 mode calculated from equation (2.8) by using the pipe data given from Table 2.1.

Since $b_s = b_w/2a$, where b_w is the width of the modal sensor, and the non-dimensional wavenumber of the n = 2 mode at the ring frequency $k_{2b} = 2\pi a/\lambda_{2r}$, where/λ_{2r} ,is the

wavelength of the n = 2 wave at the ring frequency, the criterion for determination of the width of the sensor is thus given by

$$b_w < \frac{\lambda_{2r}}{\pi} \approx \frac{1}{3}\lambda_{2r}$$

Since only the flexural wave can potentially propagate, it means that, if the width of the modal sensor is less than one third of the wavelength of the flexural wave at the ring frequency, it only senses the response of the n = 2 mode.

For the modal sensor having a shape of a sine function, the same procedure to obtain the expression of the generated charge for the cosine function shape is applied. Since

$$\sin(k_{nb} b_s \sin(p\theta)) = 2\sum_{m=1}^{\infty} J_{2m-1}(k_{nb} b_s)\sin[(2m-1)p\theta]$$

therefore,

$$q_s = 2\pi\lambda_2 b_s z_o e_{31}(n^2-1)\sum_{b=1}^{4} W_2 e^{jk_{2b}s_c} \qquad \text{for } n = 2 \text{ and } b_s \le 0.16 \qquad \ldots(3.17)$$

The total generated charge, q_t, for a mode with arbitrary orientation can be obtained by a combination of both sine and cosine function shapes of the modal sensors in terms of the square root of the sum of the squares and it is

$$\begin{aligned} q_t &= \sqrt{q_c^2 + q_s^2} \\ &= 2\pi b_s z_o e_{31}(n^2-1)\sum_{b=1}^{4} W_2 e^{jk_{2b}s_c} \end{aligned} \qquad \text{for } n = 2 \text{ and } b_s \le 0.16 \qquad \ldots(3.18)$$

The orientation angle can be determined as

$$\phi = \frac{1}{2}\tan^{-1}\left(\frac{\lambda_2}{\lambda_1}\right) = \frac{1}{2}\tan^{-1}\left(\frac{q_s}{q_c}\right) \qquad \ldots(3.19).$$

3.3 Experimental Setup and Procedure

In this section, the experiments that were carried out to validate the modal sensor equation for the semi-infinite pipe are described. Their results are also compared with those obtained when using an accelerometer to evaluate the performance of the sensor for active vibration control purposes.

Modal sensors were fabricated by cutting 52 μm thick PVDF in the shape of a sine function with $b_s = 0.009$ approximately (both sine and cosine function modal sensors are the same but there are placed at a 90^0 circumferential angle to each other on the pipe) and the poling of the patches is arranged as shown in figure 3.6. Since the PVDF sheet manufactured from Measurement Specialties, Inc, has piezoelectric strain constants, $d_{31} = 23*10^{-12}$ m/V and $d_{32} = 3*10^{-12}$ m/V, with $E_{pv} = 2*10^9$ N/m^2 and $\nu_{pv} = 1/3$, then the piezoelectric stress constants $e_{31} = 54*10^{-3}$ C/m^2 and $e_{32} = 24*10^{-3}$ C/m^2. The schematic of the experimental setup is shown in figure 3.7. The 2.7 m plastic pipe, whose properties are given in Table 2.1, was suspended by cords. It was free at one end and had an anechoic termination at another end to ensure that its behaviour was as a semi-infinite pipe. Both modal sensors shaped in sine and cosine functions were placed close together, 300 mm and 310 mm respectively from the excitation point. The pipe was excited at the free end by a small shaker, which was driven by a random signal supplied by an HP 3566A Signal Analyzer. The arrangement of the modal sensors of n = 2 mode was such that individual elements were expected to detect the in-phase response of the n = 2 mode and out-of-phase response of other modes. So the experiment first carried out was to investigate this behaviour. Because the modal sensors were expected to detect only the motion of the n = 2 mode after they were electrically connected together, an experiment was conducted to verify this and the results were used to compare with those obtained from accelerometer measurement at the same position.

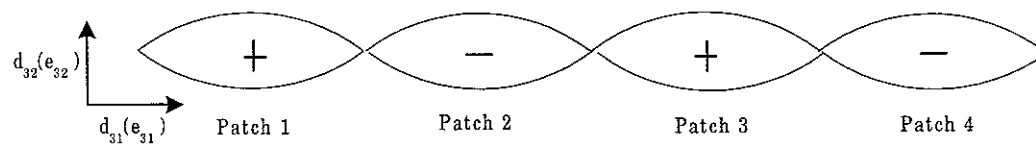

Figure 3.6: Arrangement of modal sensor

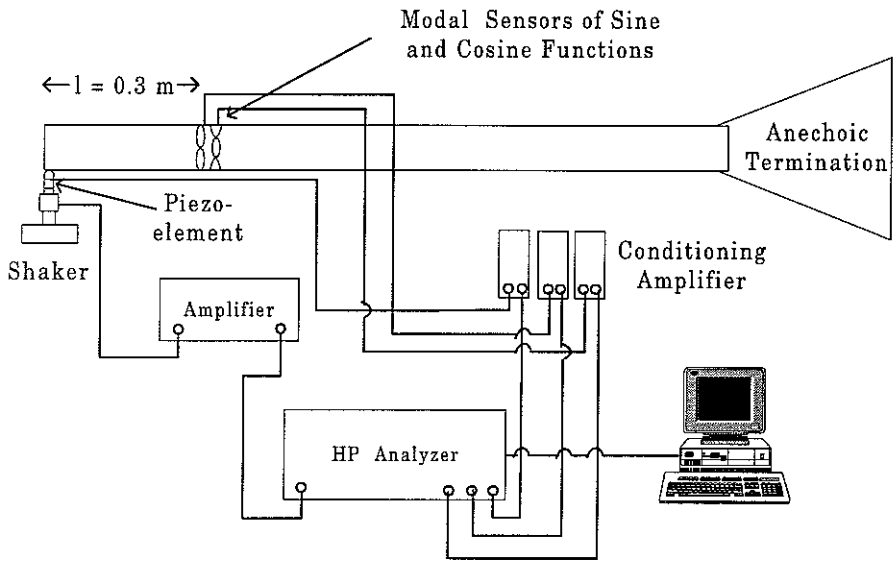

Figure 3.7: Experimental setup for evaluation of the modal sensor.

3.4 Experimental Results

In this section, experimental results are presented and compared with predictions calculated using the theory described in the previous section. The results obtained from the modal sensors are also compared with those obtained from the array of accelerometers described in the previous chapter.

The measured responses of the modal sensor were in the form of the transfer function, Coulomb/ Newton. To compare this transfer function with the theory, the receptance has to be incorporated into equation (3.18). The receptance of a semi-infinite pipe is given by equation (2.19) and is repeated here for convenience.

$$\frac{\overline{\overline{W}}_n(s=s_c,\theta)}{F_o} = -\frac{j\varepsilon_n\Omega^2[\lambda_1\cos(n\theta)+\lambda_2\sin(n\theta)]}{2\pi\omega^2\rho h a^2}\sum_{b=1}^{4}\mathrm{Re}\,s_b e^{jk_{nb}s_c} \qquad \ldots(3.20)$$

where $\varepsilon_n = 1$ for $n = 0$ and

$\varepsilon_n = 2$ for $n \geq 1$,

s_c is the non-dimensional axial location of centre of the sensor to the radius of the pipe,

$\Omega = \omega/\omega_r$ is the non-dimensional frequency,

ω_r is the ring frequency,

F_o is the amplitude of the excitation force and

$$\mathrm{Re}\,s_b = \frac{(k_{nb}^2+n^2)^2}{4k_{ab}\left[2\beta^2(k_{nb}^2+n^2)(k_{nb}^2+n^2-1)(k_{nb}^2+n^2-\frac{1}{2})+(1-\nu^2)k_{nb}^4-\Omega^2(k_{nb}^2+n^2+\frac{1}{2})\right]}$$

Since the radial displacement is given by equation (3.8) as (omitting terms of $e^{-j\omega t}$)

$$\overline{\overline{W}}_n(s=s_c,\theta) = \sum_{b=1}^{4} W_n\left(\lambda_1\cos(n\theta)+\lambda_2\sin(n\theta)\right)e^{jk_{nb}s_c},$$

the modal amplitude can be determined as

$$\sum_{b=1}^{4} W_n e^{jk_{nb}s_c} = -\frac{j\varepsilon_n\Omega^2 F_o}{2\pi\omega^2\rho h a^2}\sum_{b=1}^{4}\mathrm{Re}\,s_b e^{jk_{nb}s_c} \qquad \ldots(3.21)$$

Substituting it into equation (3.18) and dividing the both sides of the equation by the force amplitude, F_0, thus the transfer functions of the n = 2 modal sensors shaped in cosine and sine functions are

$$T_{qc} = \frac{q_c}{F_0} = -\frac{j6\lambda_1 b_s z_0 e_{31}\Omega^2}{\omega^2 \rho h a^2} \sum_{b=1}^{4} Re\, s_b e^{jk_{2b}s_c} \quad \text{and}$$

$$T_{qs} = \frac{q_s}{F_0} = -\frac{j6\lambda_2 b_s z_0 e_{31}\Omega^2}{\omega^2 \rho h a^2} \sum_{b=1}^{4} Re\, s_b e^{jk_{2b}s_c} \text{ , respectively.} \qquad \ldots(3.21\ a,b)$$

Hence, the total transfer function is

$$T_q = \frac{q_t}{F_0} = -\frac{j6 b_s z_0 e_{31}\Omega^2}{\omega^2 \rho h a^2} \sum_{b=1}^{4} Re\, s_b e^{jk_{2b}s_c} \,. \qquad \ldots (3.22)$$

In order to compare the response of the modal sensors to that of the accelerometer, it has to be converted into the form of the accelerance for the n^{th} mode. At a particular position, it is given by

$$H_n(s,\theta) = -\frac{1}{F_0}\omega^2 \overline{\overline{W}}_n(s,\theta) = -\frac{1}{F_0}\omega^2 \sum_{b=1}^{4} W_n \left(\lambda_1 \cos(n\theta) + \lambda_2 \sin(n\theta)\right) e^{jk_{nb}s} \qquad \ldots(3.23)$$

Integration over the surface area at s = s_c, the accelerance of the cosine function modal sensor for the n = 2 mode is given by

$$H_{2c}(s = s_c) = -\frac{1}{F_0}\omega^2 \lambda_1 \sum_{b=1}^{4} W_n e^{jk_{2b}s_c} \qquad \ldots(3.24)$$

Substituting equation (3.24) into equation (3.16) gives

$$H_{2c}(s = s_c) = -\frac{1}{F_0}\frac{\omega^2 q_c}{6\pi b_s z_0 e_{31}} \qquad \ldots(3.25)$$

Similar to the sine function modal sensor for the n = 2 mode, the accelerance is

$$H_{2s}(s = s_c) = -\frac{1}{F_0}\frac{\omega^2 q_s}{6\pi b_s z_0 e_{31}} \qquad \ldots(3.26)$$

Hence, the total accelerance is given by

$$H_{2t}(s=s_c)=\sqrt{H_{2c}^2+H_{2s}^2}=\frac{1}{F_0}\frac{\omega^2 q_t}{6\pi b_s z_0 e_{31}} \qquad \ldots(3.27)$$

The experimental results presented are as follows.

Figure 3.8: Frequency response of patches of modal sensor

Figure 3.9: Total amplitude of modal sensor obtaining from the root sum square of the modals sensor shaped in sine and cosine function

Figure 3.10: Orientation angle of pipe determined from modal sensor

Figure 3.11: Comparison between total response of the modal sensor and of the accelerometer array for n= 2 mode

Figure 3.12: Comparison between the frequency response of the cosine function of the modal sensor and of the accelerometer array for n= 2 mode.

Figure 3.13: Comparison between the frequency response of the sine function of the modal sensor and of the accelerometer array for n= 2 mode.

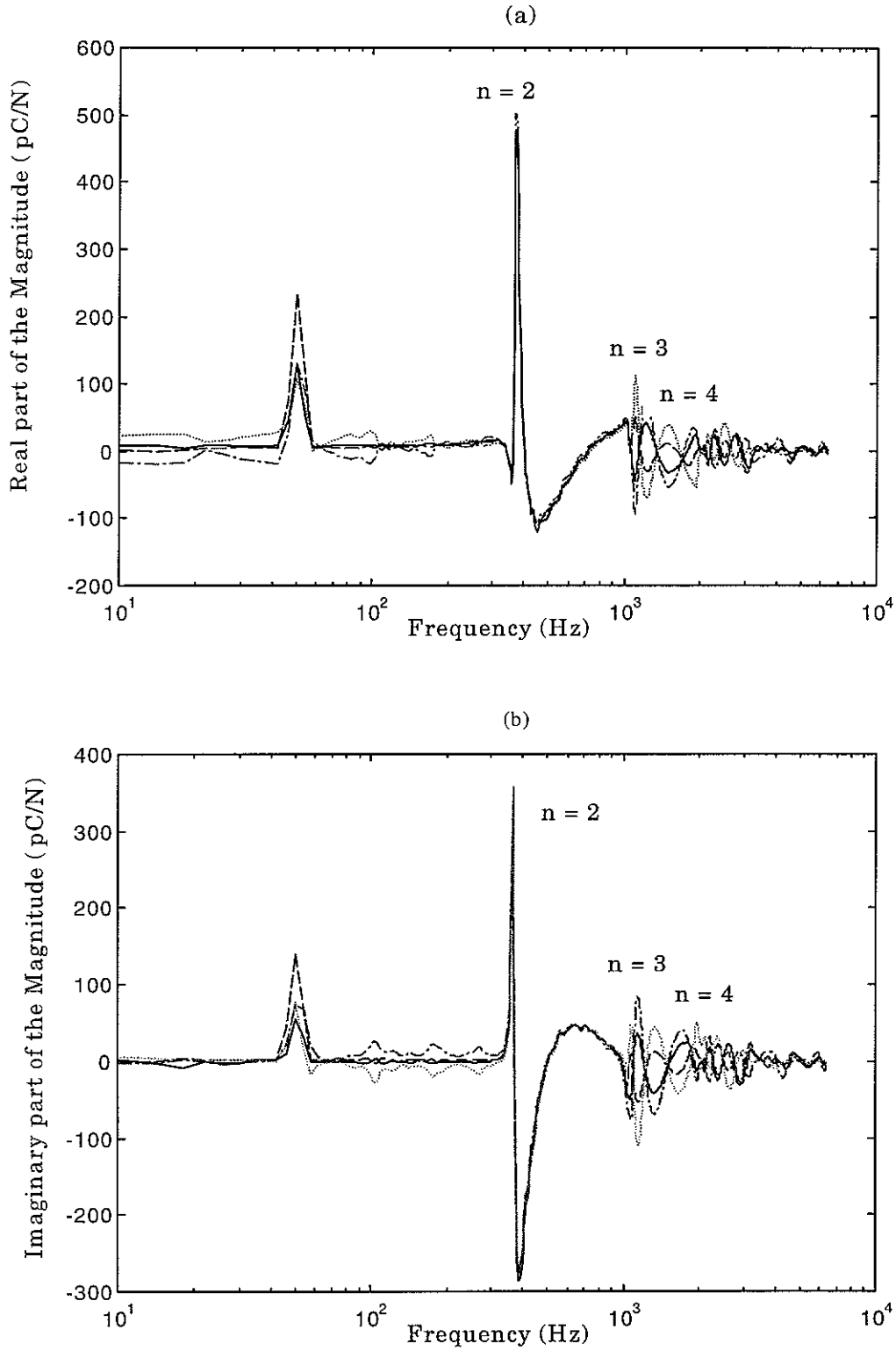

Figure 3.8: Frequency response of the individual patches of the modal sensor ; a) real part b) imaginary part: -.- patch 1; ... patch 2; ¯ patch 3; --- patch 4.

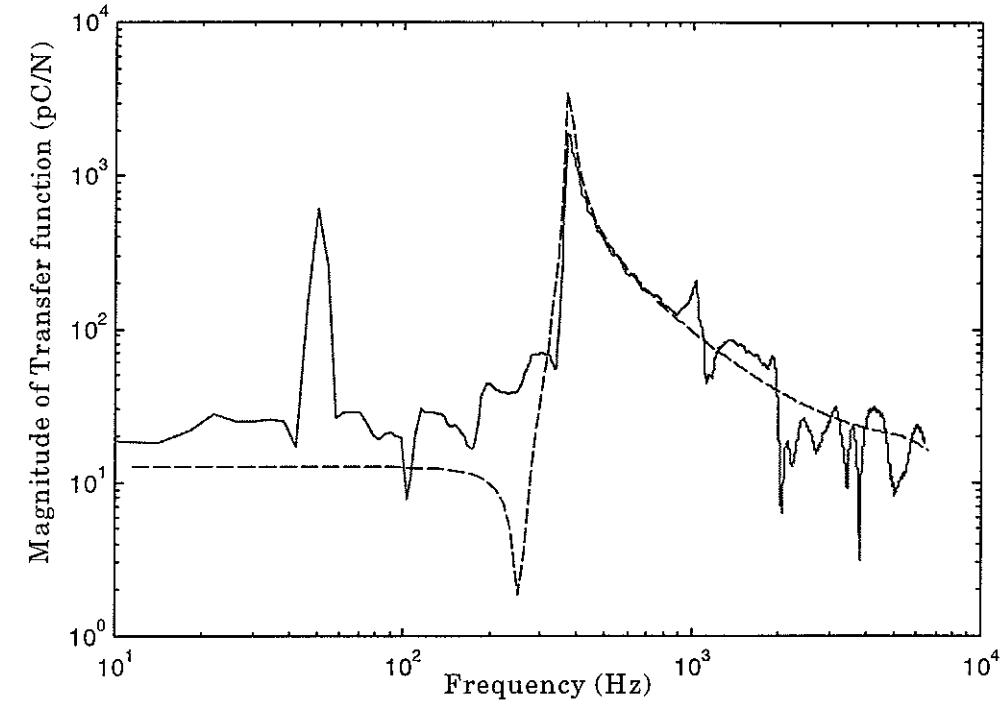

Figure 3.9: Amplitude of the response measured by the modal sensors obtained from the combination of the sine and cosine function shapes; _ measured result; --- equation (3.18)

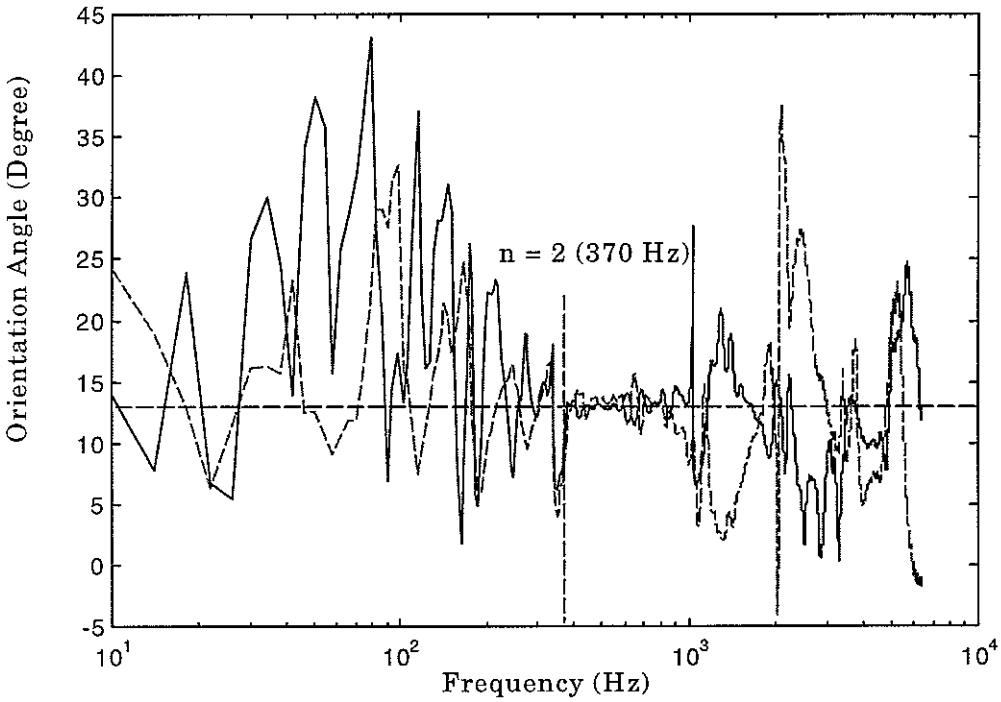

Figure 3.10: Orientation angle of the pipe with respect to the force position;— Process from accelerometer; --- Process from Modal sensors.

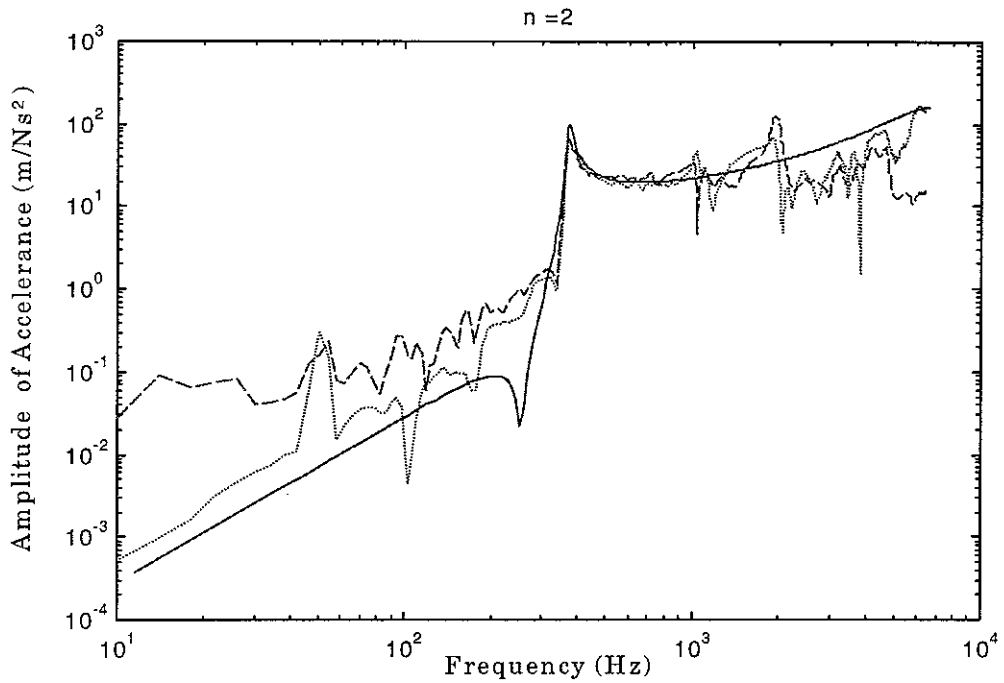

Figure 3.11: Comparison between the total response in terms of accelerance for the n= 2 mode; ... modal sensor output from equation (3.24) ; --- output of array of accelerometers without mass effect accounted for; —— equation (2.25) .

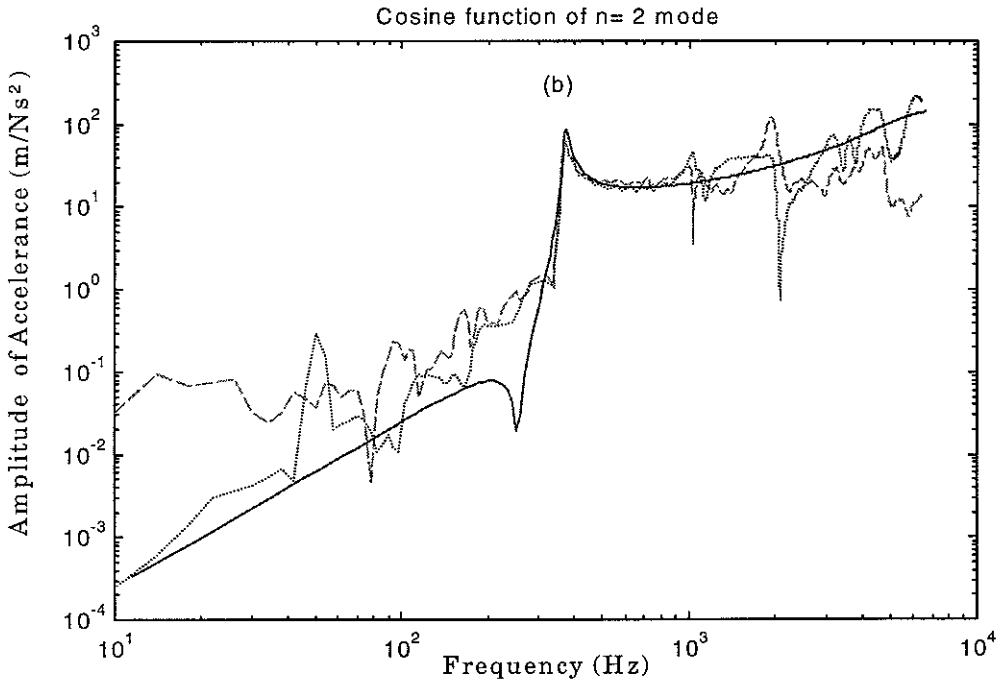

Figure 3.12: Comparison between the frequency response of the cosine function in terms of accelerance for the n= 2 mode; ... modal sensor output from equation (3.25) ; --- output of array of accelerometers without mass effect accounted for; —— equation (2.25) .

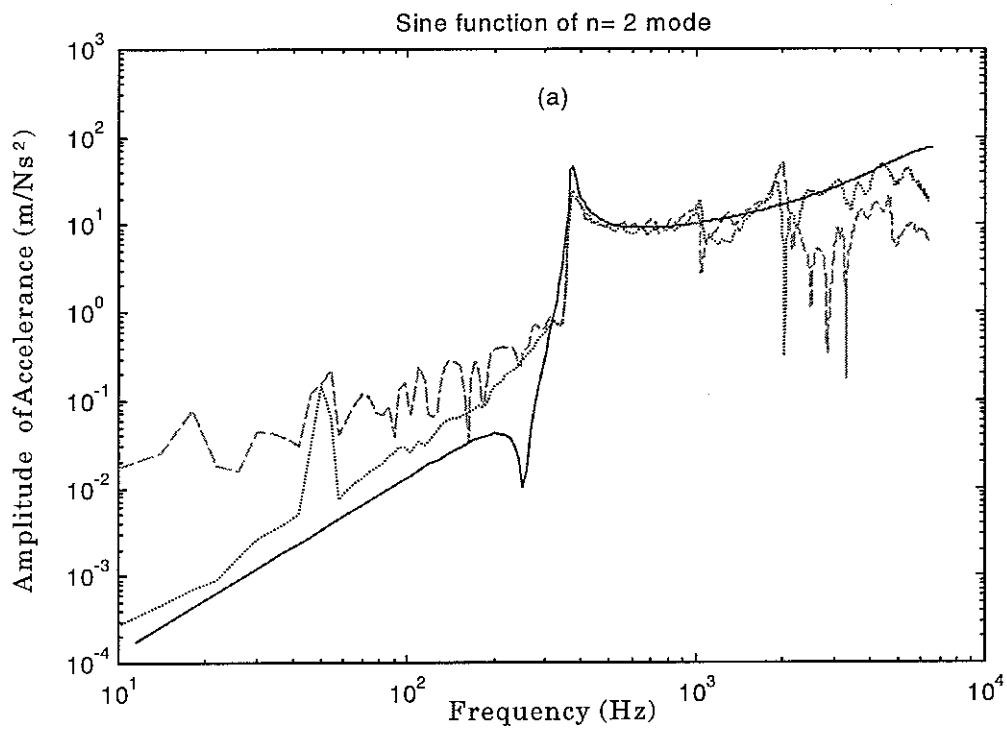

Figure 3.13: Comparison between the frequency response of the sine function in terms of accelerance for the n= 2 mode; ... modal sensor output from equation (3.26) ; --- output of array of accelerometers without mass effect accounted for;—— equation (2.25) .

3.5 Discussions

With the responses of the patches of the modal sensor shown in figure 3.8, it is clear that they are in phase in the n = 2 mode and out of phase in the other modes. This means it will only sense the motion of the n = 2 mode after the patches are electrically connected together.

The total response of the n = 2 modal sensor, which was shown in figure 3.9, agrees with the theory except at low frequencies, where the pipe is mass-like. This disagreement may also be due to inaccuracy in the shapes of the modal sensors and the significant response of the pipe at the cut-on frequencies of other modes, where there are large reflected waves.

Before the waves cut on, the pipe has very small displacements, so the orientation angle of the pipe was determined after the wave cut on (370 Hz). It was shown in figure 3.10, that the orientation obtained from the modal sensor is consistent with that obtained from the accelerometer.

Good performance of the modal sensor was shown in figures 3.11-3.13 in which the response of the modal sensor and that of the accelerometer array are compared. It illustrates that the modal sensor has a better performance than the accelerometer due to a negligible mass effect even at high frequencies. If the effect of the mass of accelerometers is removed from the experiment results, the responses obtained by both sensors are similar.

4. Conclusions

The work presented in this report is an evaluation of the modal sensor for the n = 2 mode of the pipe. Based on Flugge's shell theory, the relationship between the charge generated from a PVDF sensor and the combination of the axial and circumferential bending strains has been established for the case of in-extensional deformation. By using the Bessel function to describe the pipe strains induced on the surface of a modal sensor, it is found that the modal sensor is sensitive to higher order modes as well as the n=2 mode. This is because the circumferential strain is coupled with the axial strain via the Poisson's ratio of the pipe. If the axial strain over the surface of the modal sensor is not constant, the higher order modes can be induced on the sensor. The cross-sensitivity is dependent upon the ratio of one half of the modal sensor width to the radius of the pipe (b_s). However, if b_s is small enough to keep the axial strain constant over its surface, the modal sensor will only be sensitive to the circumferential bending strain of the pipe so that it is only sensitive to the n = 2 mode. This means that the performance of the modal sensor in detecting only the n = 2 mode increases with the decrease of its sensitivity because of its surface area reduced. It is found that to keep the axial strain of n = 2 mode constant over the frequency range of interest, the width of the modal sensor has to be less than one third of the wavelength of the flexural wave at the ring frequency and hence it only senses the response of the n = 2 mode.

The analytical model for a modal sensor has been successfully validated by experiment results. It was also compared with an accelerometer array in terms of the accelerance of the pipe. Clearly, the modal sensor provides a better performance than an accelerometer array since it does not change the mechanical properties of the structure as an accelerometer does. Even if the mass of the accelerometer is small, the motion of the pipe can dramatically changed, especially at high frequencies. Because the modal sensor is constructed from PVDF, it has very little mass and it does not affect the motion of the pipe. In addition, to measure the response of a particular mode by means of modal decomposition, an array of accelerometers has to be used and the outputs from these accelerometers has to be processed. Therefore in an active control system, a modal sensor, which only has two leads, is much more suitable than an accelerometer as a sensor for a particular mode.

5. REFERENCES

1. Leissa A. W., 1973, "Vibrations of shells", NASA SP-288, Washington DC: U.S. Gov Printing Office.

2. Lin T. C. and Morgan G. W., 1956, "Wave propagation through fluid contained in a cylindrical, elastic shell", The Journal of the Acoustical Society of America, Vol. 28, No. 6, pp. 1165-1176.

3. Fuller C. R. and Fahy F. J., 1982, "Characteristics of wave propagation and energy distributions in cylindrical elastic shells filled with fluid", J. of Sound and Vibration, Vol. 81, No. 4, pp. 501-518.

4. Fuller C.F.,1983, "The input mobility of an infinite circular cylindrical elastic shell filled with fluid", J. of Sound and Vibration, Vol. 87, No. 3, pp. 409-427.

5. Heckl M., 1962, "Vibrations of point-driven cylindrical shells", The Journal of the Acoustical Society of America, Vol. 34, No. 10, pp. 1553-1557.

6. Brennan M. J., Elliott S. J. and Pinnington R. J., Dec 1993, "Waves in fluid filled pipes", RNEC-RR-93035, Royal Naval Engineering College, Mechanics Group Research Report.

7. Balas M., 1978, "Feedback control of flexible systems", IEEE Transactions on Automatic Control, AC-23, No.4, pp.673-679.

8. Lee, C.-K., and Moon, F.C., 1990, "Modal sensors/actuators", ASME Journal of Applied Mechanics, Vol. 57, pp. 434-441.

9. Gu Y., Clark R. L., Fuller C. R. and Zander A. C., 1994, "Experiments on active control of plate using piezoelectric actuators and polyvinylidene fluoride (PVDF) modal sensors", ASME J. of Vibration and Acoustics, Vol. 116, pp. 303-308.

10. Tzou H. S., 1992, "A new distributed sensor and actuator theory for intelligent shells", J. of Sound and Vibration, Vol. 153, No. 2, pp. 335-349.

11. Tzou H. S. and Bao Y., 1996, "Parametric study of segmented transducers laminated on cylindrical shells, Part 1 : Sensor patches", ", J. of Sound and Vibration, Vol. 197, No. 2, pp. 207-224.

12. Fuller C. R. and Brevart B. J., July 1995, "Active control of coupled wave propagation and associated power in fluid-filled elastic long pipes", Active 95, pp. 3-14.

13. Callahan J. and Baruh H., 1999, "Modal sensing of circular cylindrical shells using segmented piezoelectric elements", Smart Materials and Structures, No. 8, pp. 125-135.

14. Fahy F. J., 1985, "Sound and structural vibration: radiation, transmission and response", Academic Press.

15. Brevart B. J. and Fuller C. R., 1993, "Active control of coupled wave propagation in fluid-filled elastic cylindrical shells", J. Acoust. Soc.Am., Vol. 94, No. 3, pp. 1467-1475.

16. Brennan M. J., Elliott S. J. and Pinnington R. J., 1997, "The dynamic coupling between piezoceramic actuators and a beam", J. Acoust. Soc.Am., Vol. 102, No. 4, pp. 1931-1942.

17. Lee C. K., 1990, "Theory of laminated piezoelectric plates for the design of distributed sensors/actuators. Part I: Governing equations and reciprocal relationships", J. Acoust. Soc.Am., Vol. 87, No. 3, pp. 1144-1158.

18. Flugge W., 1962, "Stresses in shells", 2nd Edn., Springer-Verlag.

19. Timoshenko S. and Woinowsky-Krieger S., 1956, "Theory of plates and shells", 2nd Edn., McGraw-Hill Book Company, INC.

20. Arfken G.,1985, "Mathematical methods for physicists", 3rd Edn., Academic Press, INC.

21. Brennan M. J., Elliott S. J. and Pinnington R. J., May 1993, "Decomposition of propagating flexural waves", RNEC-RR-93017, Royal Naval Engineering College, Mechanics Group Research Report.

22. Mead D. J., 1988, "Passive vibration control", John Wiley & Sons Ltd.

23. Timoshenko S., Young D. H. and Weaver, Jr. W., 1974, "Vibration problems in engineering", 4th Edn., John Wiley & Sons, Inc.

24. Soedel W., 1993, "Vibrations of shells and plate", 2nd Edn., MARCEL DEKKER, INC.

Appendix A: Fourier and Inverse Fourier Transform of Radial Displacement of Pipes.

A.1 Fourier Transform of Radial Displacement of Pipes

In this appendix, the derivation of a radial displacement of pipes using a spatial Fourier Transform is presented. The radial displacement of pipes as a spatial function may be expressed in terms of a wavenumber transform, $\overline{W}_o(k,\theta)$, as (Arfken [20])

$$w(s,\theta) = \frac{1}{\sqrt{2\pi}} \int_{-\infty}^{\infty} \overline{W}_o(k,\theta) e^{jks} dk \qquad \ldots(A.1)$$

Also, the wavenumber transform, $\overline{W}_o(k,\theta)$, at a particular circumferential angle of a pipe may be expressed as

$$\overline{W}_o(k,\theta) = \frac{1}{\sqrt{2\pi}} \sum_{n=-\infty}^{\infty} \overline{W}_n(k) e^{jn\theta} \qquad \ldots(A.2)$$

Since $e^{jn\theta} = \cos(n\theta) + j\sin(n\theta)$, equation (A.2) becomes

$$\overline{W}_0(k,\theta) = \frac{1}{\sqrt{2\pi}} \sum_{n=0}^{\infty} \varepsilon_n \overline{W}_n(k) \cos(n\theta) \qquad \ldots(A.3)$$

where $\varepsilon_n = 1$ for $n = 0$ and

$\varepsilon_n = 2$ for $n \geq 1$.

Substituting equation (A.3) into equation (A.1) gives

$$w(s,\theta) = \frac{1}{2\pi} \int_{-\infty}^{\infty} \sum_{n=0}^{\infty} \varepsilon_n \overline{W}_n(k) \cos(n\theta) e^{jks} dk \qquad \ldots(A.4)$$

A.2 Inverse Fourier Transform of Radial Displacement of Pipes

In this section, the relationship between a wavenumber amplitude and a spatial amplitude of a radial displacement is established by using the spatial Inverse Fourier Transform. The Inverse Fourier Transform of the wavenumber amplitude in equation (A.2) may be given by (Arfken [20])

$$\overline{W}_n(k) = \frac{1}{\sqrt{2\pi}} \int_0^{2\pi} \overline{W}_o(k,\theta) e^{-jn\theta} d\theta \qquad \ldots(A.5)$$

and the Inverse Fourier Transform of the radial displacement of a pipe as a spatial function into a wavenumber function, $\overline{W}_o(k,\theta)$, in equation (A.1) may be given by

$$\overline{W}_o(k,\theta) = \frac{1}{\sqrt{2\pi}} \int_{-\infty}^{\infty} w(s,\theta) e^{-jks} ds \qquad \ldots(A.6)$$

Substituting equation (A.6) into equation (A.5) gives

$$\overline{W}_n(k) = \frac{1}{2\pi} \int_0^{2\pi} \int_{-\infty}^{\infty} w(s,\theta) e^{-jks} e^{-jn\theta} ds d\theta \qquad \ldots(A.7)$$

The solution of radial motion in the spatial domain for an infinite pipe may be written as

$$\begin{aligned} w(s,\theta,t) &= \sum_{m=0}^{\infty} \sum_{b=1}^{8} W_{nb} \cos(m(\theta-\phi)) e^{j(k_{nb}s-\omega t)} \\ &= \sum_{m=0}^{\infty} \sum_{b=1}^{8} W_{nb} \left[\lambda_1 \cos(m\theta) + \lambda_2 \sin(m\theta)\right] e^{j(k_{nb}s-\omega t)} \end{aligned}$$

where $\lambda_1 = \cos(m\phi)$,

$\lambda_2 = \sin(m\phi)$

θ is the azimuthal angle and

ϕ is the azimuthal orientation angle,

Substituting the solution of radial motion into equation (A.7) and rearranging it give

$$\overline{W}_n(k) = \frac{1}{2\pi}\int_0^{2\pi}\sum_{m=0}^{\infty}\sum_{b=1}^{8} W_{nb}\left[\lambda_1\cos(m\theta)+\lambda_2\sin(m\theta)\right]e^{-jn\theta}d\theta\int_{-\infty}^{\infty}e^{j(k_{nb}-k)s}ds$$
$$= \int_0^{2\pi}\sum_{m=0}^{\infty}\sum_{b=1}^{8} W_{nb}\left[\lambda_1\cos(m\theta)+\lambda_2\sin(m\theta)\right]e^{-jn\theta}\delta(k_{nb}-k)d\theta \qquad \ldots(A.8)$$

where $\delta()$ is the delta function.

Since $e^{jn\theta} = \cos(n\theta) + j\sin(n\theta)$, integration of equation (A.8) by θ over a circumference of a pipe yields

$$\overline{W}_n(k) = \frac{2\pi}{\varepsilon_n}\sum_{b=1}^{8} W_{nb}(\lambda_1-\lambda_2)\delta(k_{nb}-k)$$
$$= \frac{2\pi}{\varepsilon_n}\sum_{b=1}^{8} W_{nb}\delta(k_{nb}-k)e^{-jn\phi} \qquad \ldots(A.9)$$

Appendix B: Wave Decomposition

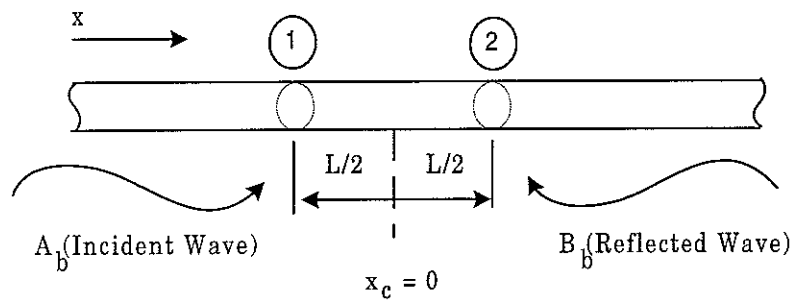

Figure B.1: Decomposition of incident and reflected waves.

Brennan et al [21] proposed a method to decompose flexural propagating waves of a beam by using an array of two sensors. The same method can be applied to decompose flexural waves of a pipe as well. In this method, two sets of measurements around the pipe are taken in the far field where there are no evanescent waves. Before the method is applied, the modal decomposition technique described in the next section is used to separate the measurement results into each mode, which may be expressed in the form of separated waves as

$$w_n = \sum_{b=1}^{4} A_b e^{jk_{nb}s} + \sum_{b=1}^{4} B_b e^{-jk_{nb}s} \qquad \ldots(B.1)$$

where A_b is the amplitude of the incident wave,

B_b is the amplitude of the reflected wave,

$s = x/a$ and

a is the radius of the pipe.

For a finite pipe, the reflected waves are generated at the termination. Since only a flexural wave can propagate in the far field, the equation (B.1) becomes

$$w_n = A_b e^{jk_{nb}s} + B_b e^{-jk_{nb}s} \qquad \ldots(B.2)$$

Then the displacement at the points 1 and point 2 are

$$w_{n1} = A_b e^{jk_{nb}(s_{xc}-l/2)} + B_b e^{-jk_{nb}(s_{xc}-l/2)},$$

$$w_{n2} = A_b e^{jk_{nb}(s_{xc}+l/2)} + B_b e^{-jk_{nb}(s_{xc}+l/2)}.$$

where x_c is the centre location between the point 1 and point 2,

$s_{xc} = x_c/a$ and

l is the distance between the point 1 and point 2,

which may be written in the form of a matrix as

$$\begin{bmatrix} e^{-jk_{nb}l/2} & e^{jk_{nb}l/2} \\ e^{jk_{nb}l/2} & e^{-jk_{nb}l/2} \end{bmatrix} \begin{bmatrix} A_0 \\ B_0 \end{bmatrix} = \begin{bmatrix} w_{n1} \\ w_{n2} \end{bmatrix} \qquad \ldots(B.3)$$

where $A_0 = A_b e^{jk_{nb}s_{xc}}$ and

$B_0 = B_b e^{-jk_{nb}s_{xc}}$.

Therefore, the amplitudes of both waves are

$$\begin{bmatrix} A_0 \\ B_0 \end{bmatrix} = \frac{j}{2\sin k_{nb}l} \begin{bmatrix} e^{-jk_{nb}l/2} & -e^{jk_{nb}l/2} \\ -e^{jk_{nb}l/2} & e^{-jk_{nb}l/2} \end{bmatrix} \begin{bmatrix} w_{n1} \\ w_{n2} \end{bmatrix} \qquad \ldots(B.4)$$

It was pointed out by Brennan et al [21] that equation (B.4) tends to ill-conditioning at the cut-on frequencies and at frequencies where integer numbers of half wavelengths are equal to the distance between the two sensors.

Appendix C: Modal decomposition

To investigate the reduction of each circumferential structural mode amplitude that is achieved by applying active vibration control, modal decomposition of the measured response should be carried out so that a comparison of the response before and after control applied to each mode can easily be undertaken. Moreover, the modal decomposition technique may be used to measure the effectiveness of a distributed PVDF modal sensor. This technique is based on the principle of discrete orthogonality (Arfken [20]). To illustrate this technique, equation (2.25) is considered and is written as

$$H_n = \frac{j\varepsilon_n \Omega^2 (\lambda_1 \cos(n\theta) + \lambda_2 \sin(n\theta))}{2\pi\rho h a^2} \sum_{b=1}^{4} Res_b e^{jk_{nb}s}$$

Since the term on the right hand side of this equation consists of two separate parameters, θ and s , the total accelerance may be written as

$$H = \sum_{n=0}^{\infty} \varepsilon_n A_n (\lambda_1 \cos(n\theta) + \lambda_2 \sin(n\theta)) \qquad \ldots(C.1)$$

where

$$A_n = \frac{j\Omega^2}{2\pi\rho h a^2} \sum_{b=1}^{4} Res_b e^{jk_{nb}s}$$

$\varepsilon_n = 1$ for $n = 0$ and

$\varepsilon_n = 2$ for $n \geq 1$.

Assuming the measurement is made using a point sensor (i.e. accelerometer) at N points around a pipe with equal angle. Then,

$$\theta = \frac{2\pi}{N} p_\theta$$

where p is the position of the measurement.

To decompose pipe modes in terms of the cosine function, both sides of equation (C.1) are multiplied by $\frac{1}{N}\cos(\frac{2\pi p_\theta}{N} m)$ and all responses measured around the pipe are summed to give

$$\frac{1}{N}\sum_{p=0}^{N-1} H\cos(\frac{2\pi p_\theta}{N}m) = \frac{1}{N}\sum_{p=0}^{N-1}\sum_{n=0}^{\infty}\varepsilon_n A_n\left(\lambda_1\cos(\frac{2\pi p_\theta}{N}n)+\lambda_2\sin(\frac{2\pi p_\theta}{N}n)\right)\cos(\frac{2\pi p_\theta}{N}m) \quad ...(C.2)$$

where m is the desired mode to be decomposed.

Using the property of orthogonality, the response of the desired mode for the cosine function can be determined as

$$\frac{1}{N}\sum_{p=0}^{N-1} H\cos(\frac{2\pi p_\theta}{N}m) = H_c = \lambda_1 A_m \quad ...(C.3)$$

To decompose pipe modes in terms of the sine function, the same procedure is applied except that both sides are multiplied by $\frac{1}{N}\sin(\frac{2\pi p_\theta}{N}m)$ instead of $\frac{1}{N}\cos(\frac{2\pi p_\theta}{N}m)$. Hence, the response of the desired mode for the sine function is

$$\frac{1}{N}\sum_{p=0}^{N-1} H\sin(\frac{2\pi p_\theta}{N}m) = H_s = \lambda_2 A_m \quad ...(C.4)$$

The total response, A_m, of the desire mode can be obtained by combining equation (C.3) and (C.4) as follows to give

$$A_m = \sqrt{H_c^2 + H_s^2} \quad ...(C.5)$$

and the orientation angle is obtained from

$$\phi = \frac{1}{m}\tan^{-1}\left(\frac{\lambda_2}{\lambda_1}\right) = \frac{1}{m}\tan^{-1}\left(\frac{H_s}{H_c}\right) \quad ...(C.6)$$

Appendix D: Effect of Mass Loading on Pipe

With an accelerometer attached, a motion of a pipe itself is changed. In this section, an effect of a mass of an accelerometer is analysed in order to obtain the actual motion of a pipe with a mass attached.

An attached mass such as an accelerometer changes the dynamic behaviour of the pipe structure. To predict the motion of the pipe with a mass attached, the effect of mass loading has to be considered. The mobility method is applied for analysis of this effect and it is schematically shown in figure D.1 in which a force, F_1, excites a pipe at the location (1) and a response of the pipe is measured by an accelerometer (Mass) at the location (2).

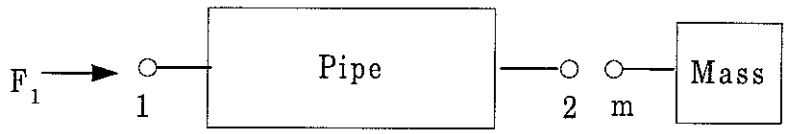

Figure D.1 : General framework of the connection between pipe and mass

Following the work done by Mead [22], the velocity at the interface between the accelerometer and the pipe at the location (2) in figure D.1 is

$$\frac{v_2}{F_1} = \frac{M_{21}}{1+\frac{M_{22}}{M_m}} \qquad \ldots(D.1)$$

where

M_{21} is the transfer mobility of pipe,

M_{22} is the point mobility of pipe and

M_m is the mobility of mass.

Since

$$M_{21} = -\sum_{n=0}^{\infty} \frac{\varepsilon_n \Omega^2 [\lambda_1 \cos(n\theta) + \lambda_2 \sin(n\theta)]}{2\pi\omega\rho\, ha^2} \sum_{b=1}^{4} Res_b e^{jk_{nb}s},$$

$$M_{22} = -\sum_{n=0}^{\infty} \frac{\varepsilon_n \lambda_1 \Omega^2}{2\pi\omega\rho\, ha^2} \sum_{b=1}^{4} Res_b \quad \text{and}$$

$$M_m = -\frac{1}{jm\omega},$$

therefore,

$$\frac{v_2}{F_1} = \frac{-\sum_{n=0}^{\infty} \frac{\varepsilon_n \Omega^2 [\lambda_1 \cos(n\theta) + \lambda_2 \sin(n\theta)]}{2\pi\omega\rho\, ha} \sum_{b=1}^{4} Res_b e^{jk_{nb}s}}{1 + \sum_{n=0}^{\infty} \frac{j\varepsilon_n m \lambda_1 \Omega^2}{2\pi\rho\, ha} \sum_{b=1}^{4} Res_b} \qquad \ldots(D.2)$$

From equation (D.2), the velocity for a particular mode at the location (2) in figure D.1 can be determined as

$$\frac{v_{2n}}{F_1} = \frac{-\frac{\varepsilon_n \Omega^2 [\lambda_1 \cos(n\theta) + \lambda_2 \sin(n\theta)]}{2\pi\omega\rho\, ha} \sum_{b=1}^{4} Res_b e^{jk_{nb}s}}{1 + \sum_{n=0}^{\infty} \frac{j\varepsilon_n m \lambda_1 \Omega^2}{2\pi\rho\, ha} \sum_{b=1}^{4} Res_b} \qquad \ldots(D.3)$$